Food and Chemical Toxicology 131 (2019) 110545

Contents lists available at ScienceDirect

Food and Chemical Toxicology

journal homepage: www.elsevier.com/locate/foodchemtox

Dietary CCPS from bitter gourd attenuates sodium arsenite induced female reproductive ailments cum infertility in wistar rats: anti-inflammatory and anti-apoptotic role

Hasina Perveen[a], Arindam Dey[a], Namrata M. Nilavar[b], Goutam Kumar Chandra[c], Syed Sirajul Islam[d], Sandip Chattopadhyay[a,*]

[a] Department of Biomedical Laboratory Science and Management, and Clinical Nutrition and Dietetics Division, (UGC Innovative Department), Vidyasagar University, Midnapore, West Bengal, 721102, India
[b] Department of Biochemistry, Indian Institute of Science, Bangalore, 560 012, India
[c] Department of Physics, National Institute of Technology Calicut, Calicut, 673 601, Kerala, India
[d] Department of Chemistry and Chemical Technology, Vidyasagar University, Midnapore, 721102, West Bengal, India

ARTICLE INFO

Keywords:
Arsenic
CCPS
Fertility and akt signaling

ABSTRACT

This investigation explored a dietary therapy of pectic polysaccharide (CCPS) (2 mg/ Kg BW) against female repro-toxicity and infertility triggered by sodium arsenite (As^{3+}) (10 mg/ Kg BW) in Wistar rats. The isolated CCPS consists of D-galactose and D-methyl galacturonate with a molar ratio of 1: 4. FTIR spectral analysis of CCPS and CCPS- sodium arsenite (As^{3+}) complex indicated a possible chelating property of CCPS in presence of binding sites (OH^-/COOH) for As^{3+}. Series of negatively charged galacturonate residues in CCPS provide better potential for cation chelation. CCPS significantly mitigated As^{3+} induced ovarian, uterine lipid peroxidation, and reactive oxygen species (ROS) generation by the restoration of superoxide dismutase (SOD), catalase and glutathione peroxidase (GPx) activities. CCPS post-treatment enhanced ovarian steroidogenesis along with a restoration of normal tissue histoarchitecture in As^{3+} fed rats by regulating the estradiol receptor alpha (ER-α). CCPS suppressed anti-inflammatory properties effectively found since a down-regulation of NF-kappa B (NF-κB), pro-inflammatory tumor necrosis-α (TNF-α) and interleukin-6 (IL-6) were observed in arsenicated rats with CCPS. This study confirmed the up-regulation of uterine pro-apoptotic/ apoptotic proteins caspase-3, poly ADP ribose polymerase (PARP), proliferating cell nuclear antigen (PCNA), phospho p53 and Bax, followed by down-regulation of Bcl-2 and protein Kinase B (AKT) signaling pathway along with uterine tissue regeneration in As^{3+} exposed rats. Oral CCPS attenuated the above apoptotic expressional changes significantly and dietary CCPS ensured successful fertility with the birth of healthy pups in lieu of infertile condition in As^{3+} fed rats. Moreover, this study also supports that CCPS treatment attenuated the As^{3+} toxicity by modulating the S-adenosine methionine (SAM) pool components, B_{12}, folate and homocysteine.

1. Introduction

The redox-active form of arsenic is highly toxic (Bode and Dong, 2002) and known to induce oxidative stress (Hartley et al., 2001). Excessive reactive oxygen spices (ROS) production also damages the cellular lipids, proteins, and DNA. Moreover, it can also alter the cellular signal transduction by changing gene expression, activation of the transcription factors, and induction of apoptosis (Pan et al., 2009). Reproductive ailments and developmental problems occur due to arsenic toxicity. Inorganic arsenic causes alteration of spermatogenesis, reductions of testosterone and gonadotrophins, and disruptions of steroidogenesis (Kim and Kim, 2015). Arsenic also affects the female reproductive cycle as it suppresses the ovarian steroidogenesis with low plasma levels of estradiol and progesterone followed by prolonged diestrous phase, degeneration of ovarian follicles and uterine cells (Zhang et al., 2000; Dash et al., 2018). Arsenic down-regulates estrogen receptor and estrogen-responsive genes (Chatterjee and Chatterjee, 2010). During pregnancy, inorganic arsenic accumulation in fetus leads to fetal death (Ahmad et al., 2001). Arsenic exposure is known to change the breast milk content of trophic factors and induces maternal morbidity (Raqib et al., 2009). It is a global challenge to control arsenic related adverse health effects. Few drugs are usually used to manage the

* Corresponding author.
E-mail addresses: sandipdoc@yahoo.com, sandipdoc@mail.vidyasagar.ac.in (S. Chattopadhyay).

https://doi.org/10.1016/j.fct.2019.05.053
Received 27 February 2019; Received in revised form 26 May 2019; Accepted 29 May 2019
Available online 01 June 2019
0278-6915/

Abbreviations

DMSA	meso 2, 3-dimercapto-succinic acid
DMPS	2, 3- dimercaptopropane sulfonic acid
BAL	british Anti Lewisite;
ROS	reactive oxygen species
CCPS	pectic polysaccharide;
CPCSEA	committee for the purpose of control and supervision of experiments on animals
FTIR	fourier transform infrared
KBr	potassium bromide;
XRD	X-ray diffraction
NMR	nuclear magnetic resonance
D2O	deuterium oxide;
ppm	parts per million
SEM	scanning electron microscope
TEM	transmission electron microscope
BW	body weight
As^{3+}	sodium arsenite;
MDA	malondialdehyde
CD	conjugated Dienes
NPSH	non protein soluble thiol
SOD	superoxide dismutase
GPx	glutathione peroxidase
LDH	lactate dehydrogenase
ELISA	enzyme-linked immune sorbent assay
Hcy	homocysteine;
LH	luteinizing hormone
FSH	follicle-stimulating hormone
NF-κB	nuclear factor kappa-light-chain-enhancer of activated B cells
MT-1	metallothionein-1
IL-6	interleukin-6
TNF-α	tumor necrosis factor alpha
ER- α	estradiol receptor alpha
MPA	metaphosphoric acid
EDTA	ethylenediamine tetra acetic acid
HPLC	high-performance liquid chromatography
NAD	nicotinamide adenosine dinucleotide;
DHEA	dehydroepiandrosterone
HSD	hydroxysteroid dehydrogenase
BSA	bovine serum albumin
NADP	nicotinamide adenine dinucleotide phosphate
SDS PAGE	sodium dodecyl sulfate-polyacrylamide gel electrophoresis;
PVDF	Polyvinylidene difluoride;
PBST	phosphate buffered saline with 0.1% Tween 20
AKT	protein Kinase B
PARP	poly ADP ribose polymerase
PCNA	proliferating cell nuclear antigen
PCR	polymerase chain reaction
cDNA	complementary DNA
GAPDH	glyceraldehyde 3-phosphate dehydrogenase

arsenic mediated toxicity in humans but long time use causes moderate to severe adverse effects (Carleton et al., 1948; Inns et al., 1990). In recent years plant extracts of *Terminalia arjuna* (Maity et al., 2018) *Emblica officinalis* (Maiti et al., 2014) and *Moringa oleifera* (Chattopadhyay et al., 2010), are reported to potentiate its protective effects on model animals by scavenging free radicals and modulation of antioxidant defense system. The antioxidants flavonoids, phenols and other phenolic compounds of *Momordica charantia* can react with the free radicals and ultimately terminates the free radical chain reaction (Kumar et al., 2010). *Momordica charantia* is known to inhibit stress-induced lipid peroxidation in rats by elevating the levels of reduced glutathione and catalase activity (Chaturvedi, 2009). Currently, investigators isolated polysaccharides from the different part of fruits and vegetables to employ its ROS scavenging action against the superoxide and hydroxyl radicals (Panda et al., 2015). It has been demonstrated that polysaccharides from *Momordica charantia* (bitter melon: Cucurbitaceae) have traditionally been used in India and other parts of the Indian subcontinent due to its various biological and therapeutic activities (Jilka et al., 1983; Panda et al., 2015; Mohammad, 2017; Mohammad et al., 2016). It contains several phenolic compounds with antioxidant activities that stimulate the immune system (Panda et al., 2015; Mohammad et al., 2016). Recently, it has been studied that polysaccharides of *Momordica* is useful in exerting its hypolipidemic effect via the regulation of peroxisome proliferators-activated α-receptor (PPARα) gene expression (Chao and Huang, 2003). Our earlier study confirmed that pectic polysaccharide (CCPS) from *Momordica charantia* has different positive action on hepatic organ against arsenic induced toxicity *in vitro* (Perveen et al., 2017). This investigation is an extension of our previous experiment (Perveen et al., 2017) with an *in vivo* approach. In this study, we focus on a possible mechanism of action of oral/dietary CCPS of *Momordica charantia* in the mitigation of arsenic induced metabolic and female reproductive organs' hazards and fertility.

2. Materials and methods

2.1. Isolation and purification of CCPS

Green karela (Bitter gourd, *Momordica charantia*) fruits were cut into small pieces and boiled for 10 h. The extract was kept overnight at 4 °C, filtered using linen cloth and centrifuged for 40 min at 8000 rpm. The supernatant was mixed with ethanol to precipitate the polysaccharide. The precipitated polysaccharide was collected through centrifugation followed by the washing with ethanol and allowed to freeze dry (Maji et al., 2012). The crude polysaccharide was purified and isolated through Sepharose-6B to obtain D-galactose and D-methyl galacturonate with a molar ratio 1: 4 (Panda et al., 2015). The structure of the obtained CCPS by the above procedure is shown below.

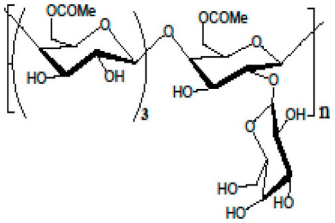

2.2. Preparation of CCPS-As^{3+} complex

CCPS (0.2 gm) was mixed in 100 ml of As^{3+} solution of concentration 1.0 ppm using magnetic stirring for 1 h. The sample was collected after filtration through Whatman syringe filter (0.2 μm) and allowed to freeze dry for characterization.

2.3. UV–vis spectroscopic measurements

The UV–vis spectrophotometric measurements were carried out using Evolution 201 UV–Vis-spectrophotometer (Thermo Fisher Scientific, Shanghai, China). The absorption spectrum of each sample solution was determined over the range of 180–500 nm.

2.4. FTIR spectroscopic measurements

The FTIR spectra were recorded using the KBr pellets in an FTIR spectrophotometer (Perkin spectrum two FTIR system, model Spectrum two) between 400 and 4000 cm^{-1}.

2.5. X-ray diffraction (XRD) measurements

XRD measurements of CCPS and CCPS-As^{3+} complex were performed using the D8 ADVANCE system. Dry powder was deposited on the sample holder and analysis was performed in the temperature range of 10–90 °C.

2.6. ^1H NMR spectroscopic measurements

CCPS and CCPS-As^{3+} complex were exchanged with deuterium via lyophilizing it with D_2O for several times and dissolved in it at room temperature for 3 h prior to NMR measurement. ^1H NMR spectra of the samples were recorded using Bruker Avance DPX-300 spectrometer (Rheinstetten, Germany) recorded at δ 4.60 ppm at 27 °C.

2.7. SEM and TEM measurements

Morphologies of CCPS and CCPS-As^{3+} complex were determined using a scanning electron microscope (SEM). For SEM measurements, one drop of sample was placed on a glass slide and allowed to evaporate under vacuum. The dried samples were deposited onto a thin gold layer and the images were taken using a ZEISS EVO 18 at an accelerating voltage of 5 kV.

More precise morphologies of the samples were obtained using transmission electron microscope (TEM) (CM-200, Philips) at an accelerating voltage of 200 kV. A small droplet (0.1%) of the samples were added on a carbon-coated copper grid and allowed to lyophilize for several hrs before TEM measurements.

2.8. Animals selection and treatment

Groups	Treatment schedule
Group 1	Control, treated normal drinking water
Group 2	As^{3+} (10 mg/kg BW), treated orally (1-8) days
Group 3	CCPS (2 mg/kg BW), treated orally (9-16) days
Group 4	As^{3+} (10 mg/kg BW), treated orally (1-8) days + CCPS (2 mg/kg BW), treated orally (9-16) days
Group 5	As^{3+} (10 mg/kg BW), treated orally (1-8) days + Dimercaptosuccinic acid (DMSA) (50 mg/kg BW), treated orally (9-16) days

Wistar female rats (90 ± 10 gm) were used in this experiment. The animals were maintained according to the CPCSEA guidelines. Prior to treatment the estrous cycle pattern of these rats were synchronized orally by a single dose (1.0 μg/kg BW) of ethinyl estradiol (Dash et al., 2018). Different stages of estrous cycle pattern were noted during the treatment. On the day of sacrifice, rats were initially anesthetized by ketamine HCl to collect blood and organs. Finally over dosing of barbiturate was used for euthanasia following the standard protocol of the institutional ethical guidelines (Ethical clearance no- IEC/11/7-Met/16).

2.9. Vaginal and cytological examination of esterous cycle

The vaginal examination of estrous cycle pattern was primarily assessed by observing the appearance of vaginal surface (Champlin et al., 1973). Vaginal smears were further studied for confirmation. The vaginal smears of all rats were collected from vagina by a sterile dropper containing normal saline. The vaginal fluid was placed on glass slide and allowed to dry prior to Leishman staining and finally examined under a light microscope (400X magnifications) (Khatun et al., 2018).

2.10. Measurement of oxidative stress serum lactate dehydrogenase (LDH)

The uterine and ovarian malondialdehyde (MDA), conjugated diens (CD) and non protein soluble thiol (NPSH) were performed as described earlier (Maity et al., 2018; Devasagayam et al., 2003; Kumar, 2012; Mieyal et al., 2008). The spectrophotometric assay of uterine and ovarian enzyme activities of superoxide dismutase (SOD), catalase and glutathione peroxidase (GPx) were assessed by following the previous reported methods (Dash et al., 2018; Pattichis et al., 1994; Hadwan, 2016; Paglia and Valentine, 1967) using Evolution 201 UV–Vis-spectrophotometer (Thermo Fisher Scientific, Shanghai, China). The serum LDH activity was measured by LDH assay (P–L) Kit from Coral Clinical Systems (Tulip Diagnostics Pvt. Ltd, Goa, India).

Further evaluated SOD, catalase, and GPx protein expression in 12% or 8% native gel and serum LDH in 8% agarose gel as described previously (Dash et al., 2018; Weydert and Cullen, 2010; Lewis et al., 2006; Liu et al., 2006; Brandt et al., 1987). Densitometric analysis was performed using Image J software.

2.11. Enzyme linked immune sorbent assay (ELISA)

Serum levels of vitamin $B_{12,}$ folate, homocysteine (Hcy), luteinizing hormone (LH), follicular stimulating hormone (FSH), and estradiol were measured by following the principle of competitive-ELISA according to the procedures recommended by the manufacturers (Wuhan Fine Biological Technology Co., Ltd., Wuhan, China). Sandwich ELISA was used to determine uterine NF kappa-B (NF-κB), estradiol receptor alpha (ER-α), and liver metallothionine-1 (MT-1) (Wuhan Fine test, China), Uterine interleukin-6 (IL-6) and serum tumor necrosis factor alpha (TNF-α) (Ray Biotech, Georgia, USA).

2.12. Serum vitamin-C preparation and HPLC measurements

Following the centrifugation, a clear supernatant part was mixed with metaphosphoric acid (MPA) in ethylenediamine tetra acetic acid (EDTA) and kept chilled and centrifuged for 10 min at 16,000g. Filtrate was used for analysis of vitamin-C by reverse phase high-performance liquid chromatography (HPLC) using C_{18} column (Robitaille and John, 2016).

2.13. Assay of ovarian steroidogenic enzymes

The ovary was homogenized in chilled buffer using spectroscopic grade glycerol. Nicotinamide adenosine dinucleotide (NAD) and dehydroepiandrosterone (DHEA) were added to the supernatant. The activity of Δ^5,3β hydroxysteroid dehydrogenase (HSD) was measured at 340 nm against a reagent blank (Talalay, 1962). For 17β-HSD the supernatant was mixed with bovine serum albumin (BSA), testosterone, and nicotinamide adenine dinucleotide phosphate (NADP) and measured against a blank at 340 nm (Jarabak et al., 1962).

2.14. Western blot

The uterine cell lysates were electrophoresed on 8% sodium dodecyl sulfate-polyacrylamide (SDS PAGE) and transferred onto polyvinylidenedifluoride (PVDF) membrane (Millipore, Darmstadt, Germany). The blots were blocked with 5% skimmed milk except the blot for phospho-p53. A 5% BSA in PBST (phosphate buffered saline with 0.1% Tween 20) was used for phospho-p53 as blocking solution. Blots were incubated with primary antibodies of Caspase 3 (Cell

Signaling Technology, Danvers, MA, USA), phospho-p53, Bax, and Bcl-2 (Santa Cruz Biotechnology, USA), protein Kinase B (AKT), (Cell signaling technology), poly ADP ribose polymerase (PARP) and, proliferating cell nuclear antigen (PCNA) (Calbio). After incubation secondary antibodies (1:10 000 in 0.1% PBST; Santa Cruz Biotechnology) were added into the blots. Blots were developed using enhanced chemilumniscence substrate (Immobilon TM western; Millipore) and the images were captured by LAS 3000 gel documentation system (FUJI, Tokyo, Japan).

2.15. Isolation of uterine mRNA and semi-quantitative polymerase chain reaction (PCR)

RNA isolation (Promega) kit was used for mRNA extraction using 90 mg of uterine tissue. mRNA was dissolved in RNase-free water and subjected to complementary DNA (cDNA) synthesis (Himedia) and used for standard PCR amplification using PCR master mix (Qiagen, Germany). The cDNA was amplified using the following primer sequences:

Target Genes	Forward primer (5′3-′)	Reverse primer (5′3-′)
BAX	5′GATCGAGCAGAGAGGATGGC3′	5′CAGTCCAAGGCAGCAGCAGGAA3′
P53	5′CTACTTCCCAGCAGGGTGT3′	5′AAAGTCTGCCTGTCGTCCAG3′
NF-κB	5′CAGACACCTTTGCACTTGGC3′	5′GCCTCCACCAGCTCTTTGAT3′
TNF-α	5′GATCGGTCCCAACAAGGAGG3′	5′CTCCAAAGTAGACCTGCCCG3′
GAPDH	5′GGGAAACCCATCACCATC 3′	5′CCCTGTTGCTGTAGCCAT3′

Glyceraldehyde 3-phosphate dehydrogenase (GAPDH) was used as a loading control (Tan et al., 2014; Kang et al., 2013). Used cDNA acts as a template and the reaction was processed at 94 °C for 5 min. Then 5 μl of each PCR product was mixed with 5 μl of loading buffer and finally loaded on agarose gel (2% w/v). The visualized DNA bands were detected using the Model GS-700 Imaging Densitometer and Molecular Analyst software (Version 1.5; Bio-Rad).

2.16. Uterine-ovarian histopathology

The uterine and ovarian tissue sections were fixed in formaldehyde. Tissues were then embedded in paraffin and 5.0 μm of thick sections were obtained and then stained with Harris-haematoxylin and eosin. Histological changes were confirmed under a microscope (magnification 100X, Olympus, Agra, India).

2.17. Breeding of animals and delivery of dietary CCPS

Four weeks old male rats and virgin female rats were obtained from the authorized animal provider and supplied with normal rat chow. Ninth week onwards a group of female rats were administrated with 10 mg/ Kg BW of As^{3+} for 8 days and allowed for mating for next 8 days. Another group was treated with arsenic in similar fashion and on 9th day onwards female rats were fed with normal chow mixed with 2.0 mg CCPS/ Kg BW for another 8 days and at the same time and duration, these groups of rats were allowed to mate. Placebo group was delivered with CCPS only at the time of mating. Control rats were supplied with vehicle only and allowed to mate in same way. The pregnant mothers started to deliver pups after 22 days. Number of successful deliveries, pup's weight and still birth with deformities were noted.

2.18. Data analysis

The statistical significance of the differences of these variables between treated cases and controls were evaluated using the post hoc Dunnett test. Differences of data (Mean ± SE, N = 6), $p < 0.05$ were considered as statistical significant.

3. Results

3.1. UV–vis spectroscopic analysis

UV-spectrum of CCPS (Fig. 1A. a) showed an absence of peak whereas its corresponding combination with As^{3+} showed two narrow but sharp peaks (Fig. 1A. b).

3.2. FT-IR spectroscopic analysis

Fig. 1B depicts the FTIR spectra of the CCPS and CCPS-As^{3+} complex in the range of 400-4000 cm^{-1}. Four important regions were identified and categorized in order to analyze the FTIR spectra of the samples under study. These regions are shown below:

i) **3000–3600 cm^{-1}** (O–H stretch region),
ii) **2800–3000 cm^{-1}** (C–H stretch region),
iii) **800–1500 cm^{-1}** (the finger print region) and
iv) **< 800 cm^{-1}.**

The strong and broad characteristic absorption bands at 3575 and 3170 cm^{-1} of CCPS are attributed to the hydroxyl (O-H) groups (Chokboribal et al., 2015; Chawananorasest et al., 2016). Two other bands around 2931 and 2368 cm^{-1} are attributed to the alkyl C–H bond in the sugar ring (Santhiya et al., 2002; Romdhanea et al., 2017). These results are consistent with our present findings. The characteristic C–H band could be due to the presence of the methyl ester group (OCH3) (1B.a). Two observed bands between 1760–1730 and 1650–1600 cm^{-1} are primarily attributed to the ester carbonyl group (C-O) and unesterified carboxylate ions (COO^-) respectively (Chatjigakis et al., 1998; Manrique and Lajolo, 2002). A study revealed that the weak band at 1736 cm^{-1} corresponds to the characteristic C = O stretching vibration of the carboxylic group of galacturonate acid and the strong band between 1650 and 1600 cm^{-1} corresponds to the aromatics C = O and C = C vibrations (Paula et al., 1998). Our results are similar and in well agreement with the findings reported in the previous literatures (Cheng et al., 2013) (1B.a). The spectral features observed in the FTIR spectrum of CCPS in the fingerprint region (800-1500 cm^{-1}) are mostly attributed to the vibrational state of the glucose monomer. The region 1300-1500 cm^{-1} corresponds to the vibrational modes related to the bending and deformations of groups containing carbon and hydrogen atoms (Deeyai et al., 2013). In the FTIR spectrum of CCPS, the vibrational band at 1248 cm^{-1} assigned to the C-O-H deformation mode (1B.a). Another vibrational band at 1160 cm^{-1} is believed to be attributed to the coupling modes of C–O and C–C stretching. The α- and β-conformers of carbohydrates could be distinguished on the basis of vibrational modes in the anomeric region from 750-1000 cm^{-1} (Xu et al., 2009). Where the absorption bands around 891 and 844 cm^{-1} are well known for the α-conformer and β-conformer respectively (Cunha et al., 2017). As shown in Fig. (1B b**),** the FTIR spectrum of the complex between sodium arsenite and CCPS confirmed the similar spectral pattern is typical for this CCPS with similar characteristics. The spectrum of CCPS-As^{3+} complex were also dominated by a broad band at the same region consisting of the stretching vibration modes of O-H groups, inter molecular hydrogen bonding and C-O groups (carboxyl and carbonyl groups). The absence of the characteristic peaks at 1541 cm^{-1} in the FTIR spectrum of CCPS indicating that it was free from protein (Zhang et al., 2018).

3.3. XRD analysis

CCPS structure did not show a diffused region corresponding to the

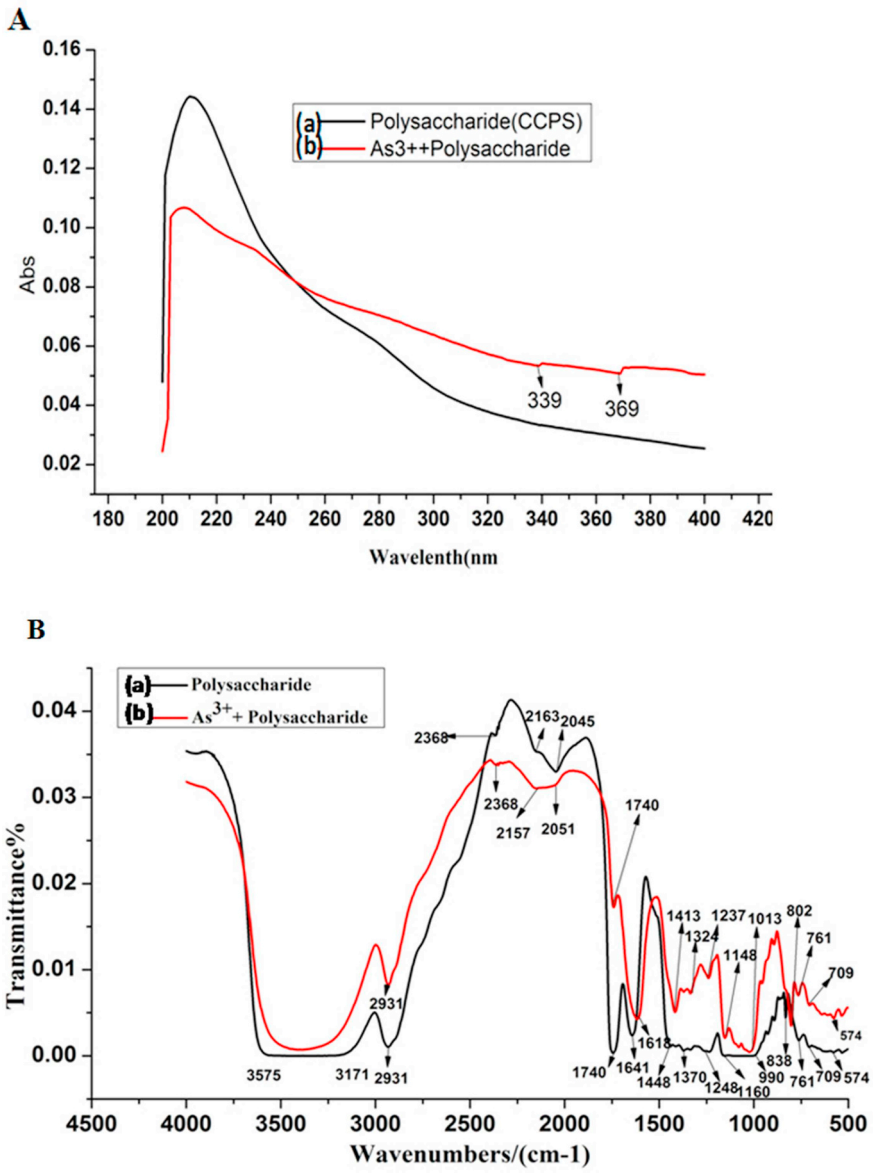

Fig. 1. A. Pattern of UV spectrogram. UV spectrogram of (a) CCPS and (b) As^{3+} + CCPS.
B. Structural analysis of CCPS and As^{3+} + CCPS. (a) Fourier transform infrared (FTIR) spectroscopy of CCPS and (b) Fourier transform infrared (FTIR) spectroscopy of As^{3+} + CCPS.

maximum value of the diffraction when X-ray passed through this CCPS (Fig. 2A). But the qualitative spectrum of CCPS-As^{3+} complex indicates the presence of arsenic and it was widely presented in the chelated samples (Fig. 2B).

3.4. ^{1}H NMR spectral analysis of CCPS

We used the ^{1}H NMR spectrum for the analysis of CCPS structure. The signals in the regions 5.50–4.90 and 4.90–4.30 ppm are attributed to the α-anomers and β-anomers protons (Corsaro et al., 2005) and confirmed that α-glycosidic and β-glycosidic linkages existed in CCPS backbone. Signals in the range of 5.12-4.90 ppm in CCPS and CCPS-As^{3+} complex (Fig. 3A and B) spectra were attributed to galacturonate acid residues (Peng et al., 2012)

3.5. Characterization by SEM & TEM

Primarily SEM study highlighted the difference between CCPS and CCPS-As^{3+} complex (Fig. 4A and B) and was further confirmed from the diffraction image of the TEM studies (Fig. 4C and D). Black spots of TEM image were due to the presence of the metalloid in CCPS (Fig. 4C). The circle along with the white spot (Fig. 4D) ensured the association between CCPS and As^{3+}. We found the corresponding planes of the arsenic (included in CCPS): where smaller circle and larger circles correspond to (102) and (212) planes in arsenic respectively.

3.6. General observation

On the day of sacrifice, we observed a significantly stunted growth

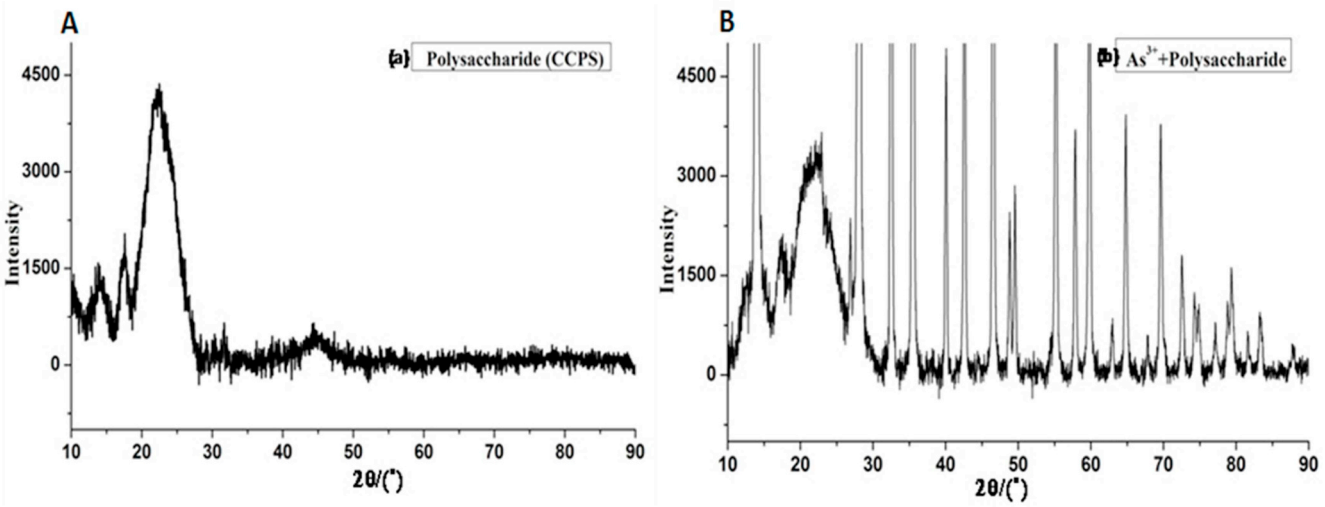

Fig. 2. Pattern of X-ray diffraction spectroscopy. (a) XRD of CCPS, and (b) XRD spectroscopy of As^{3+} + CCPS.

of ovary but uterine growth was unaltered (Table 1). Post treatment of CCPS exhibited a partial but significant recovery of ovarian uterine weight (Table 1). There was no statistical difference of body weight found between the groups (Table 1).

Vaginal smear exhibited a persistent diestrous in arsenicated animals and was significantly tend towards a synchronized estrous cycle pattern (Proestrous > Estrous > Metestrous > Diestrous) following the post treatment of CCPS (Fig. 5).

3.7. Effect of CCPS on ovarian and uterine lipid peroxidation and oxidative stress and serum LDH

In the present study, uterine and ovarian MDA and CD levels were significantly increased and the NPSH was significantly reduced in As^{3+} treated group as compared to the control group (Table 2). However, CCPS could play a corrective role in restoring the level of NPSH and end products of ovarian and uterine lipid peroxidation (MDA and CD) (Table 2).

The uterine and ovarian SOD, catalase and GPx activities were significantly diminished by the application of As^{3+} as compared to the control group (Table 2). Post-treatment of CCPS showed a significant counteraction against this alteration of antioxidant enzymes activities in As^{3+} fed rats (Table 2). We further evaluated the changes of these enzyme expressions by native gel electrophoresis. Band intensity of uterine-ovarian SOD, catalase, and GPx (Fig. 6A, B and 6C) significantly reduced following As^{3+} ingestion as compared to the control rats. Whereas, CCPS post-treatment rats significantly increased the expression of above enzymes in As^{3+} treated rats (Fig. 6A, B and 6C).

Serum LDH is considered to detect the extent of the cellular damage. Spectrophotometric (Fig. 7A) evaluation showed a significant elevation of this enzyme following As^{3+} exposure and electrozymographic imaging confirmed a higher expression of LDH as documented by the appearance of an intense band of LDH (Fig. 7B). However, CCPS in As^{3+} ingested group partially but significantly reduced the leakage of serum LDH activity with a development of a feeble band (Fig. 7B). So, we suggest that CCPS is possibly related to the protection of the cell from arsenic mediated damage or death.

3.8. Status of measured vitamins and homocysteine level

As^{3+} significantly diminished the levels of vitamin B_{12} and folic acid along with a surge of vitamin C with respect to the control groups

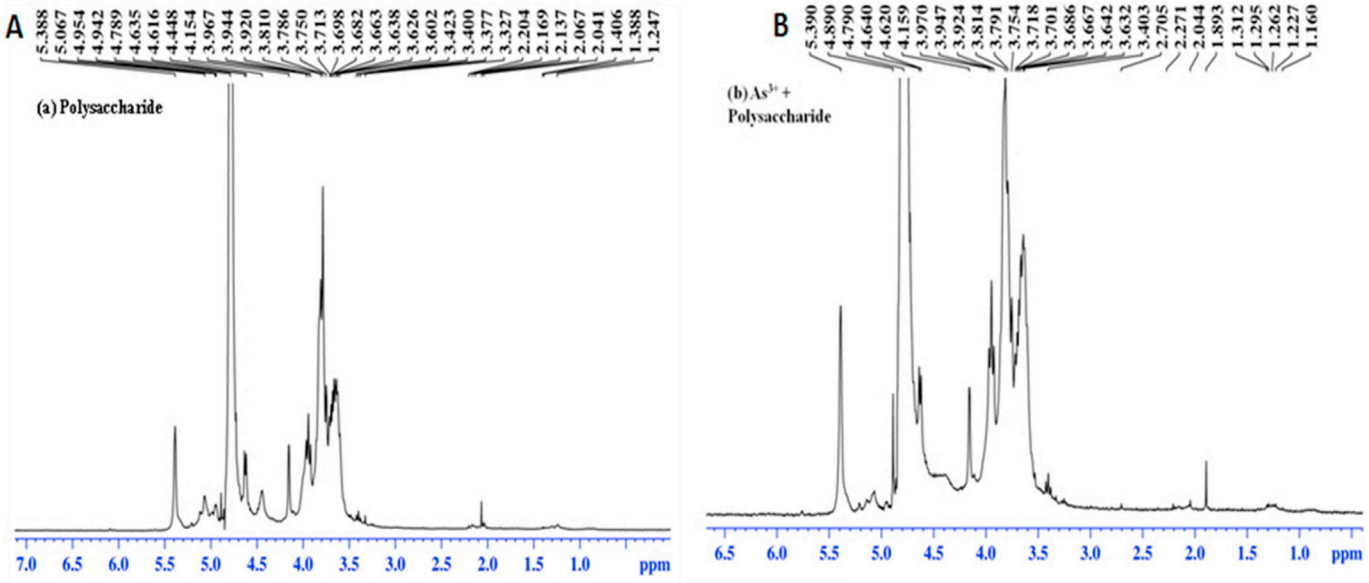

Fig. 3. NMR spectrum analysis (a) ^{1}H NMR CCPS and (b) ^{1}H NMR Polysaccharide of As^{3+} + CCPS.

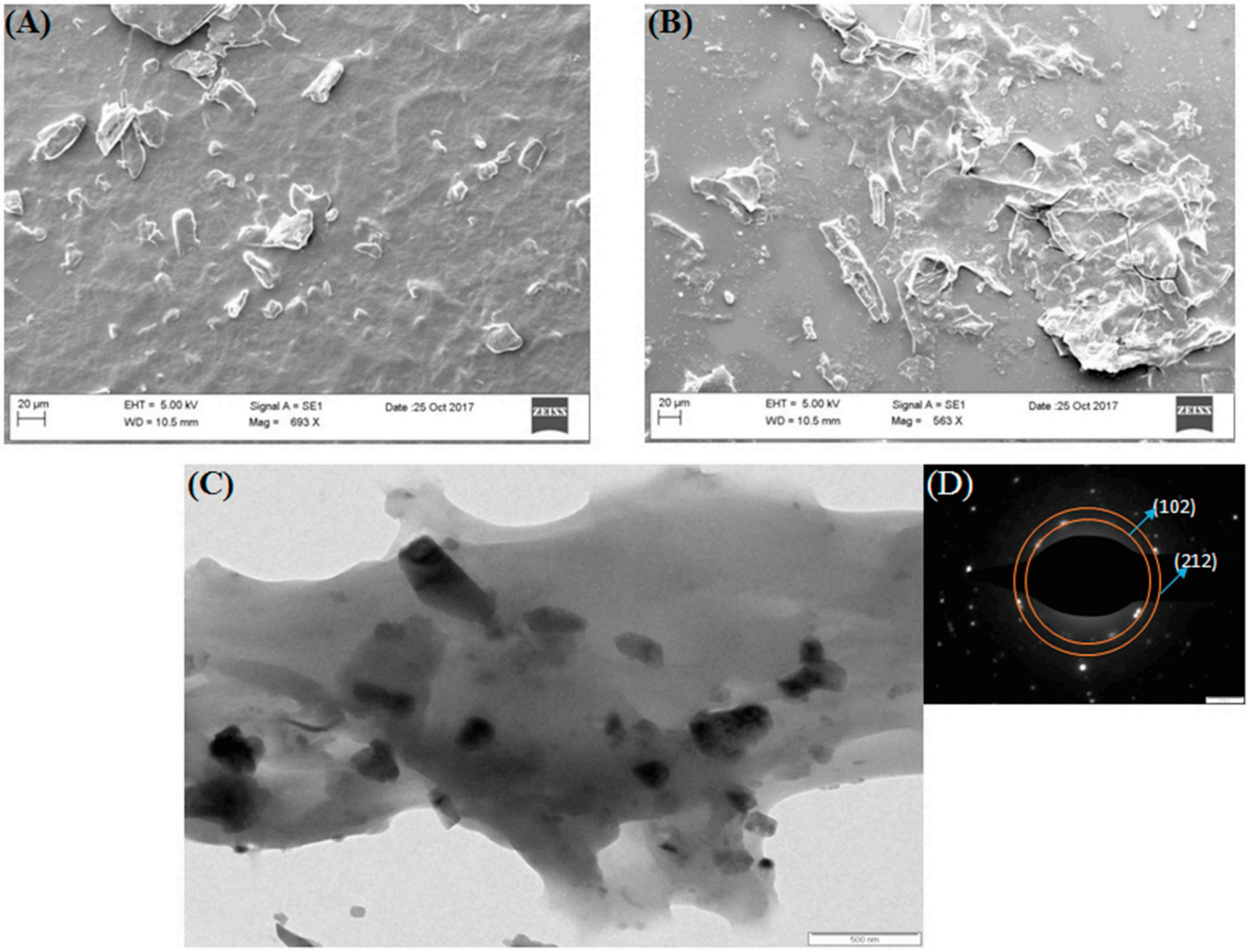

Fig. 4. Electron microscopic analysis of CCPS and As^{3+} + CCPS. (A) Scanning electron microscopey of CCPS, (B) Scanning electron microscopey of As^{3+} + CCPS association, (C) Transmission electron microscopy of As^{3+} + CCPS association and (D) Diffraction image of As^{3+} + CCPS association.

(Table 3). CCPS post-treatment in As^{3+} exposed rats significantly replenished these vitamins B_{12} and folic acid along with a further surge of vitamin C. As^{3+} noticeably raised the circulating level of Hcy (Table 3) and CCPS post-treatment in the As^{3+} exposed rat significantly suppressed this elevation of Hcy compared to the As^{3+} treated rats (Table 3). These results indicated a possible arsenic detoxification by CCPS involving these above components of SAM.

3.9. Effect on ovarian steroidogenesis and ER-α receptor

The activities of key ovarian regulatory enzymes 17β-HSD and Δ^5, 3β-HSD were meaningfully inhibited by As^{3+} when compared to the control group (Table 4). As^{3+} also suppressed estradiol, LH, and FSH levels which are the key regulators of the estrous cycle (Table 4). CCPS post treatment to As^{3+} exposed rats reverted back this steroidogenic disorder (Table 4). On the other hand, the uterine activation of ER-α receptor sensing was significantly repressed in arsenicated rats and CCPS in As^{3+} fed rats significantly reorganized the sensing of this

Table 1
CCPS changes the body growth of rats and changes the reproductive organ (uterus-ovary) indices in arsenic treated rats. These results were represented as mean ± SE, N = 6 by ANOVA followed by post hoc Dunnett test. Significant differences were expressed as *p < 0.05 with the control group and #p < 0.05 with the arsenic group.

Groups	Initial body weight (g)	Final body weight (g)	Ovary in pair (mg%)	Uterus in pair (mg%)
Control	83.1 ± 4.93	98.1 ± 3.06	0.058 ± 0.005	0.187 ± 0.021
As^{3+}	86.6 ± 4.21	93.5 ± 5.09	0.041 ± 0.003*	0.141 ± 0.047
CCPS	90.4 ± 6.83	88.9 ± 6.98	0.057 ± 0.002#	0.216 ± 0.012
As^{3+} + CCPS	87.4 ± 7	89.5 ± 8.06	0.056 ± 0.002#	0.198 ± 0.014
As^{3+} + DMSA	84.3 ± 5.02	92.6 ± 5.45	0.054 ± 0.003#	0.177 ± 0.016

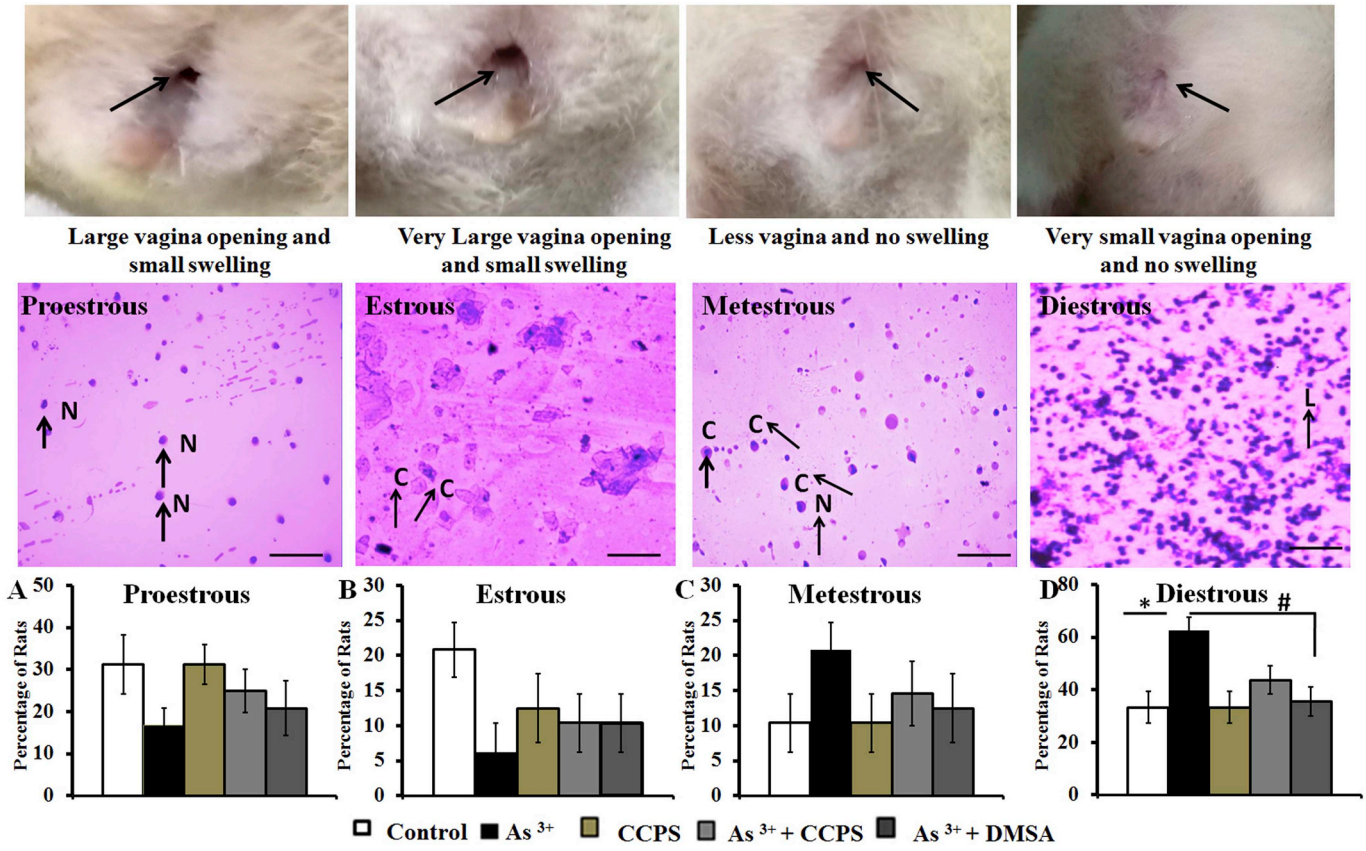

Fig. 5. Represent the curative effects of As^{3+} and CCPS on different pattern of estrous phase. At proestrous phase numerous numbers of nucleated cells **(N)** are present. In estrous phase only confined epithelial cells are observed **(C).** At metestrous phase, few leukocytes **(L),** confined epithelial cells **(C)** along with few nucleated cells **(N)** are present. At diestrous phase mostly leukocytes **(L)** are observed. The scale bar in the cytological examination is represents 50 mm. These results were represented as mean ± SE, N = 6 by ANOVA followed by post hoc Dunnett test. Significant differences were expressed as *p < 0.05, with the control group and at #p < 0.05 with the arsenic group.

Table 2
CCPS cure the oxidative stress markers (MDA, CD and NPSH) and antioxidant enzymes (SOD, catalase and GPx) activities in arsenic treated rats. These results were represented as means ± SE, N = 6 by ANOVA followed by post hoc Dunnett test. Significant differences were expressed as *p < 0.05, **p < 0.01, ***p < 0.001 with the control group and #p < 0.05, ##p < 0.01, ###p < 0.001 with the arsenic group.

Uterus			
Groups	MDA (nmol/mg of tissue)	CD (nmol/mg of tissue)	NPSH (μg/g protein)
Control	15.95 ± 1.59	12.14 ± 1.27	60.6 ± 2.8
As^{3+}	35.58 ± 3.35**	22.54 ± 2.82*	38.8 ± 0.76*
CCPS	20.04 ± 2.4#	9.88 ± 1.14##	70.6 ± 6.13###
As^{3+} + CCPS	23.61 ± 3.79	13.86 ± 1.28#	65.4 ± 1.21##
As^{3+} + DMSA	30.2 ± 2.22*	19.56 ± 0.97*	54.2 ± 4.06#
Ovary			
Control	8.66 ± 0.32	8.44 ± 0.36	31.6 ± 0.83
As^{3+}	14.24 ± 0.27***	23.38 ± 0.21***	19 ± 2.08**
CCPS	7.44 ± 0.19###	8.5 ± 0.36###	32.4 ± 1.93##
As^{3+} + CCPS	9.88 ± 0.27##	12.54 ± 0.45*###	29.8 ± 2.27#
As^{3+} + DMSA	10.12 ± 1.19#	17.69 ± 1.63***##	22.31 ± 2*
Antioxidant Profile of Uterine tissue			
Groups	SOD (U/ mg protein)	Catalase (U/ mg protein)	GPx (U/ mg protein)
Control	6.74 ± 0.59	12.42 ± 1.65	8.12 ± 0.49
As^{3+}	1.92 ± 0.35*	3.7 ± 0.55**	2.34 ± 0.26***
CCPS	10.08 ± 1.51*###	18.52 ± 1.03*###	10.16 ± 0.44###
As^{3+} + CCPS	7.32 ± 0.47#	14.76 ± 1.83###	9.86 ± 0.57###
As^{3+} + DMSA	5.98 ± 0.66#	7.72 ± 0.71	6.9 ± 0.6###
Antioxidant Profile of Ovarian tissue			
Control	6.64 ± 0.37	7.2 ± 0.29	3.9 ± 0.18
As^{3+}	1.36 ± 0.15***	2.85 ± 0.27***	1.11 ± 0.18***
CCPS	9.14 ± 0.32*###	12.87 ± 0.37***###	5.56 ± 0.31*###
As^{3+} + CCPS	7.8 ± 0.35###	10.97 ± 0.47**###	4.68 ± 0.36###
As^{3+} + DMSA	5.7 ± 0.71###	7.16 ± 0.88###	3.7 ± 0.34###

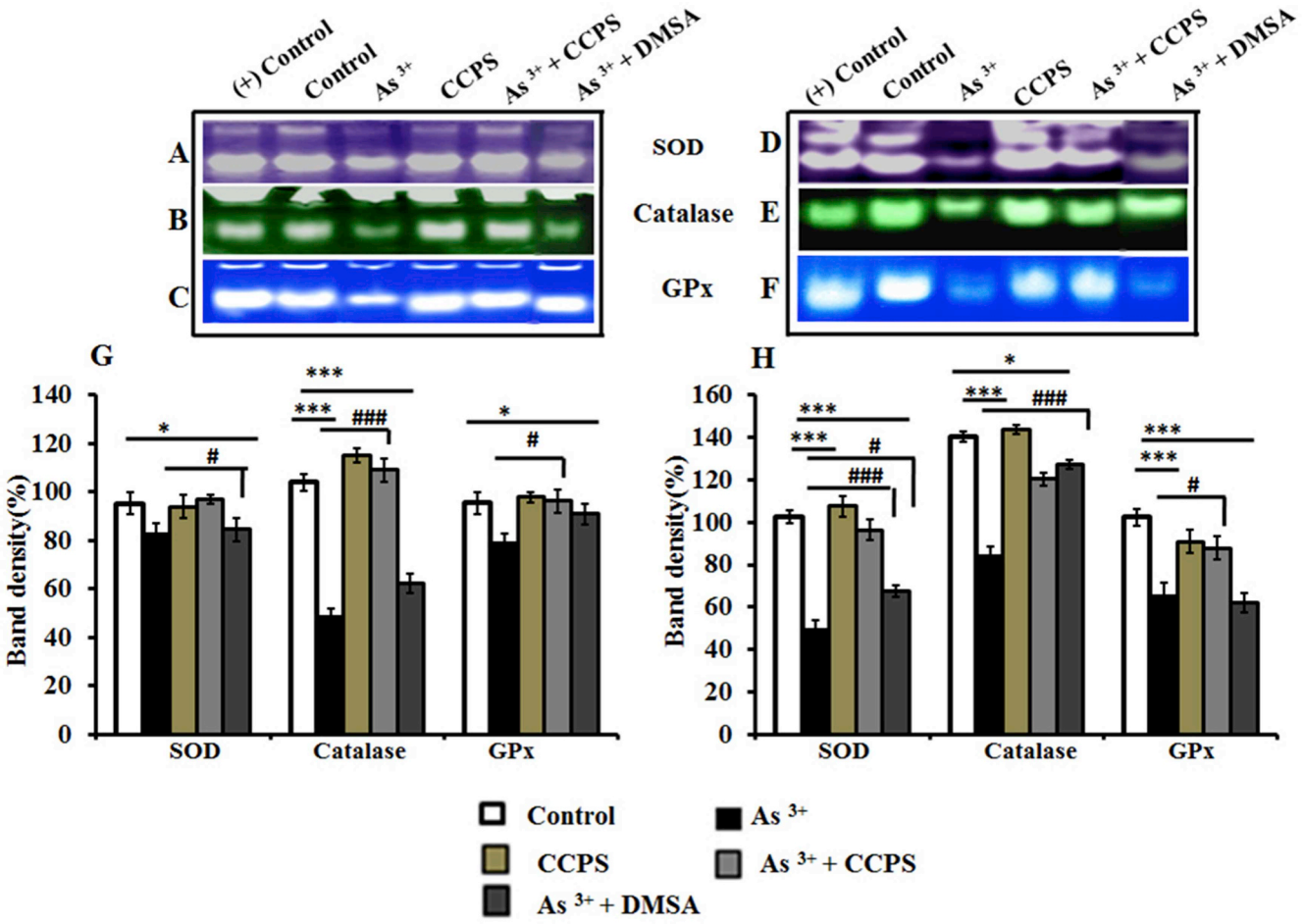

Fig. 6. Curative effects of CCPS in arsenic treated rats on uterine and ovarian enzyme activities (SOD, catalase and GPx). Antioxidant activities were performed on native gel electrophoresis (data shown 6A, 6B, and 6C respectively). The relative band density percentage (%) of positive control (+ control) with these enzymes (SOD, Catalase, and GPx) were expressed using ImageJ software and data respectively shown in 6D. These results were represented as mean ± SE, N = 6 by ANOVA followed by post hoc Dunnett test. Significant differences were expressed as *p < 0.05, ***p < 0.001 with the control group and at #p < 0.05, ###p < 0.001 with the arsenic group.

receptor molecule towards a considerable level (Table 4).

3.10. Inflammatory markers and liver MT-1 level

Increased release of uterine IL-6, NF-κB, serum TNF-α and hepatic MT-1 were attained following As^{3+} treatment in rats (Fig. 8). CCPS reduced this elevated inflammatory response in As^{3+} exposed rats along with a restoration of MT-1 towards control level (Fig. 8).

3.11. Effect of CCPS on protein expression levels in uterus

The immune blot expression pattern is depicted in Fig. 9. An over expression of uterine Bax, phospho p53, caspase-3, PARP and PCNA were observed in arsenicated rats followed by a suppressed expression of Bcl-2 and AKT (Fig. 9). Oral post administration of CCPS significantly down-regulated the protein expression of Bax, phospho p53, caspase-3, PARP and PCNA whereas significantly up-regulated Bcl-2 and AKT protein expression in the uterine tissue of As^{3+} ingested rats (Fig. 9).

3.12. Effect of CCPS on gene expression levels in uterus

In order to validate the effect of CCPS against As^{3+} on the genomic expression of Bax, p53, NF-κB, and TNF-α in uterus, the expressions were checked at the RNA transcript level. As shown in Fig. 10, semi-quantitative PCR established an up regulation of uterine Bax, p53, NF-κB, and TNF-α following As^{3+} treatment as compared to the control uterus (Fig. 10). Oral application of CCPS in the post arsenicated phase eventually showed a marked down regulation of these bio-markers (Fig. 10).

3.13. Ovarian and uterine histopathology

Fig. 11B showed that the uterine layers (perimetrium, myometrium, and endometrium) were degenerated with a considerable loss of secretory glands in As^{3+} treated rats. Post ingestion of CCPS markedly modulated the degenerating layers with an increased number of secretory glands (Fig. 11C and D). On the other hands, the As^{3+} treatment resulted in the reduced the number of growing and graafian follicles with an extensive follicular atresia in ovary (Fig. 11G). Post treatment of CCPS, however, partially but significantly recovered the ovary from above condition in arsenicated animals by increasing the number of growing follicles and reducing the number of atretic follicles (Fig. 11H and I).

3.14. Pups survival

As^{3+} consumed pregnant rats' body weight was significantly reduced in contrast to control (Fig. 12C). Control, CCPS placebo and CCPS supplemented groups in pregnant rats successfully delivered healthy pups without any death (Fig. 12D, E, 12F) when As^{3+} treated pregnant

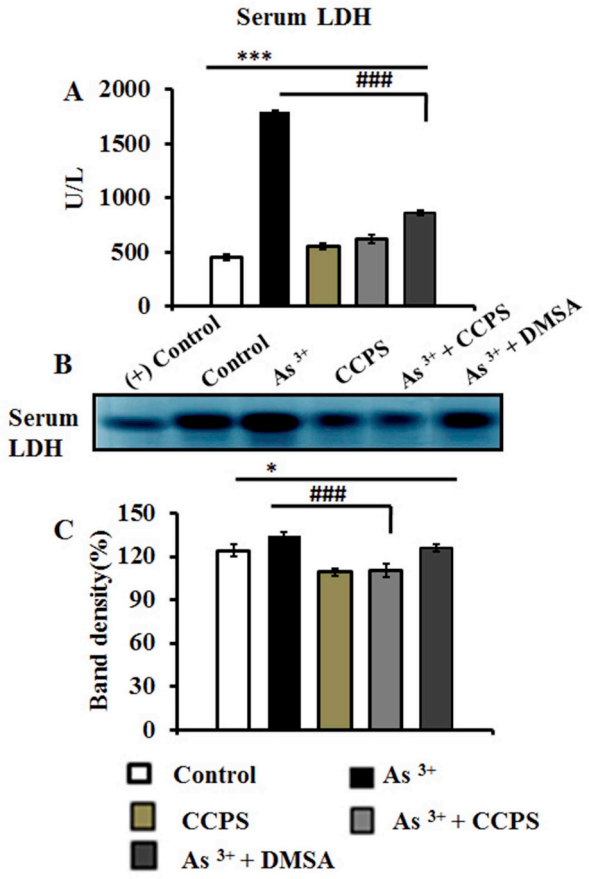

Fig. 7. Curative effect of CCPS in arsenic treated rats on Serum LDH activity. The spectrophotometry data shows that the LDH activity was improved by CCPS in arsenic treated rats (7A). The serum LDH activity was performed on agarose gel electrophoresis. CCPS reduced the serum LDH activity in arsenic treated rats (7B). The relative band density percentage (%) of positive control (+control) of serum LDH (7C) were expressed using image J software. These results were represented as mean ± SE, N = 6 by ANOVA followed by post hoc Dunnett test. Significant differences were expressed as *p < 0.05, ***p < 0.001 with the control group and at ###p < 0.001 with the arsenic group.

rats showed a significantly decline in the birth rate (Fig. 12D, E, 12F). Moreover, arsenicated pregnant rats delivered dead pups with low birth weight and a considerable number of pups were born with deformities and died immediately after birth (Fig. 12D, E, 12F) & (Fig. 12A).

4. Discussion

The present study highlights the curative efficacy of CCPS of *Momordica charantia* against arsenic-induced female organs' oxidative stress, apoptosis, inflammatory response and adverse pregnancy outcome in rats. This study is an extension of our previous study where we established an anti-oxidative role of CCPS using an *in-vitro* model (Perveen et al., 2017). Here, in this study, initially we tested the *in-vitro* binding capacity of CCPS with As^{3+} along with its characterization. Next, we demonstrated the curative action of orally administered CCPS *in-vivo* and investigated the anti-oxidative, anti-inflammatory and anti-apoptotic efficacy at protein and genomic level. Finally, we investigated the dietary efficacy of CCPS in the mitigation of adverse pregnancy outcome due to As^{3+}.

Our study is also supported by Zhang et al. regarding CCPS where they found no peaks at 180–260 nm of UV spectra and interpreted the absence of protein in CCPS (Zhang et al., 2018). This also confirmed the purity of our extracted CCPS as the present study followed the same methodology for CCPS extraction reported by one of our co-author earlier (Panda et al., 2015). In the FTIR spectrum, the spectral changes like peak shifts and intensity changes are important for inferring the interaction between two molecules. The comparison between the peak positions, i.e., the peak shift in the absorption bands of the bare molecule (CCPS) with respect to the complex molecule (CCPS-As^{3+} complex) indicates the interactions and reactions involving the related functional groups. In particular, the infrared peaks observed in the spectrum of free CCPS at 1641, 1448, 1370, 1248 and 1160 cm^{-1} (Fig. 1B a) in our study. As shown in this figure the same peaks for the CCPS-As^{3+} complex found in 1618, 1413, 1324, 1237 and 1148 cm^{-1}, respectively (Fig. 1B b). All these bands showed a drift of down-shift of 11-46 cm^{-1} in case of CCPS-As^{3+} complex as compared to free CCPS. These enormous shifts in the peak positions indicate the involvement of the carbonyl, carboxyl and hydroxyl functional groups during the interaction between CCPS and As^{3+}. The changes in intensity also observed along with the shift in these band positions. The shift in the IR absorption bands accompanied by changes in intensity in association with the functional groups suggests the direct interaction of sodium arsenite with the moieties of these functional groups of CCPS. These spectral changes indicate the possible metal chelating or the formation of graft material and the possible reactive sites of the CCPS. In CCPS structure, a series of negatively charged galacturonate acid residues have excellent potential for cation chelation (El-Zoghbi and Sitohy, 2001). An absence of the diffuse regions for CCPS obtained from XRD analysis further indicates the purity of this CCPS. A possible chelation of As^{3+} with CCPS might be confirmed from the diffused nature of qualitative spectrum of XRD (Fig. 2a). But the qualitative spectrum of CCPS-As^{3+} complex (Fig. 2b) indicates presence of As^{3+} and also its presence in the chelated samples. Moreover, ^{1}H NMR spectrum of CCPS confirms the existence of α-anomers and β-anomers/ α-glycosidic and β-glycosidic linkages with substantive glucuronic acid residues (Peng et al., 2012).

Arsenic alters different biological pathways and produces oxidative stress in organs (Agrawal et al., 2014). The antioxidant enzymes SOD and catalase have mutual importance for the elimination of ROS from different organs. SOD catalyzes the superoxide-dismutation to H_2O_2 and finally it is removed by catalase (Usoh et al., 2005). MDA is a direct product of lipid peroxidation, which is the most commonly used indicator of the severity of lipid peroxidation and a marker of oxidative stress in the uterus. Here we observed a significant decrease in the uterine and ovarian SOD, catalase and GPx activity along with a

Table 3
CCPS reduces the circulating level of serum B_{12}, folic acid and increased the level vitamin- C and homocysteine in arsenic treated rats. These results were represented as mean ± SE, N = 6 by ANOVA followed by post hoc Dunnett test. Significant differences were expressed as *p < 0.05, ***p < 0.001 with the control group and ##p < 0.01, ###p < 0.001 with the arsenic group.

Groups	B_{12} (ng/ml)	Folic acid (ng/ ml	Vitamin-C (mg/ ml)	Homocysteine (pmol/ ml)
Control	23.91 ± 3.51	1189 ± 7.33	79.2 ± 3.16	3.72 ± 0.58
As^{3+}	10.06 ± 0.71*	706.4 ± 16.23***	148.29 ± 1.63***	12.75 ± 1.5***
CCPS	70.77 ± 4.37***###	1409.2 ± 12.4***###	300.15 ± 7.07***###	2.56 ± 0.35###
As^{3+} + CCPS	64.8 ± 3.43***###	1274.4 ± 17.23*###	287.62 ± 4.91***###	4.2 ± 0.2###
As^{3+} + DMSA	38.6 ± 3.1*###	915 ± 19.7***###	202.8 ± 9.09***###	6.4 ± 0.66##

Table 4
CCPS reduces the serum hormonal level of LH, FSH and Estradiol in arsenic mediated rats in comparison with the control rats and protects the ovarian steroidogenic key enzymatic activities (17 β-HSD and Δ^5, 3-β-HSD). CCPS improves the uterine ER-α level. These results were represented as mean ± SE, N = 6 by ANOVA followed by post hoc Dunnett test. Significant differences were expressed as *p < 0.05, ***p < 0.001 with the control group and at #p < 0.05, ##p < 0.01, ###p < 0.001 with the arsenic group.

Groups	LH (mIU/ml)	FSH (mIU/ml)	Estradiol (pg/ml)
Control	7.63 ± 0.47	20.25 ± 1.33	774.8 ± 3.77
As^{3+}	1.82 ± 0.33*	5.44 ± 1.1*	110.4 ± 3.84***
CCPS	16.86 ± 1.15***###	27 ± 3.39###	1008.2 ± 2.99***###
As^{3+} + CCPS	10.82 ± 1.59###	21.55 ± 3.49##	889 ± 1.98***###
As^{3+} + DMSA	8.98 ± 0.89##	15 ± 0.89#	648 ± 1.52***###
Groups	17 β-HSD (unit/ mg of tissue)	$\Delta^{5,}$ 3 β-HSD (unit/ mg of tissue	Estradiol Receptor-α (ng/ml)
Control	24.4 ± 1.22	42.4 ± 1.22	16.37 ± 0.55
As^{3+}	9.64 ± 1.43*	25 ± 1.52***	7.85 ± 0.42***
CCPS	88.8 ± 2.74***###	44.6 ± 2.01###	27.51 ± 0.97*###
As^{3+} + CCPS	83.8 ± 4.21***###	41.8 ± 2.55##	25.06 ± 0.76*###
As^{3+} + DMSA	47.2 ± 2.42***###	35.2 ± 2.55#	19.59 ± 0.92*###

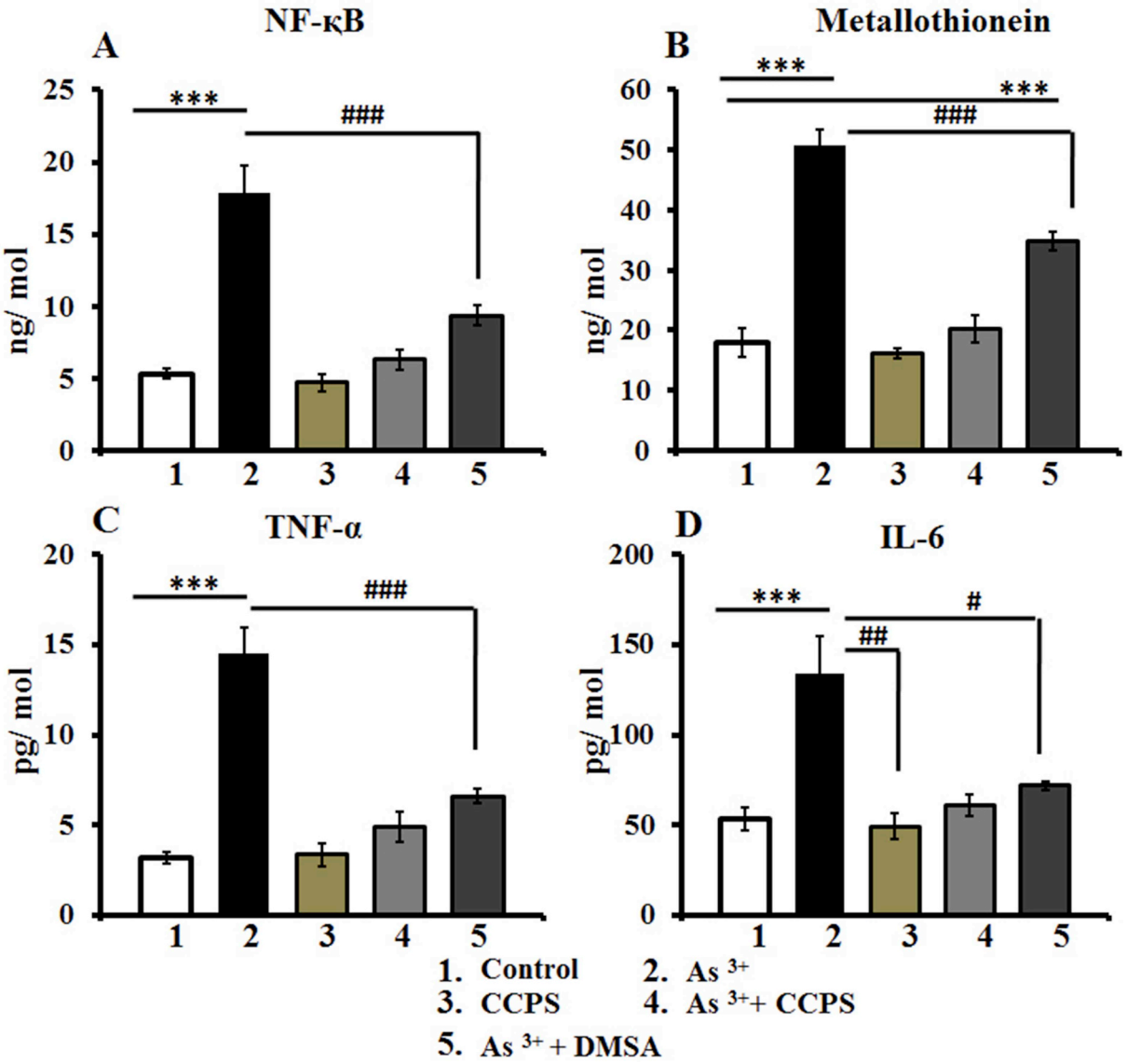

Fig. 8. The uterine NF- κB, and IL-6, serum TNF-α, and liver MT-1 level were diminished by arsenic treatment, but CCPS restored these pro-inflammatory and inflammatory cytokines of uterine tissue and liver tissue. These results were represented as mean ± SE, N = 6 by ANOVA followed by post hoc Dunnett test. Significant differences were expressed at ***p < 0.001 with the control group and #p < 0.05, ##p < 0.01, ###p < 0.001 with the arsenic group.

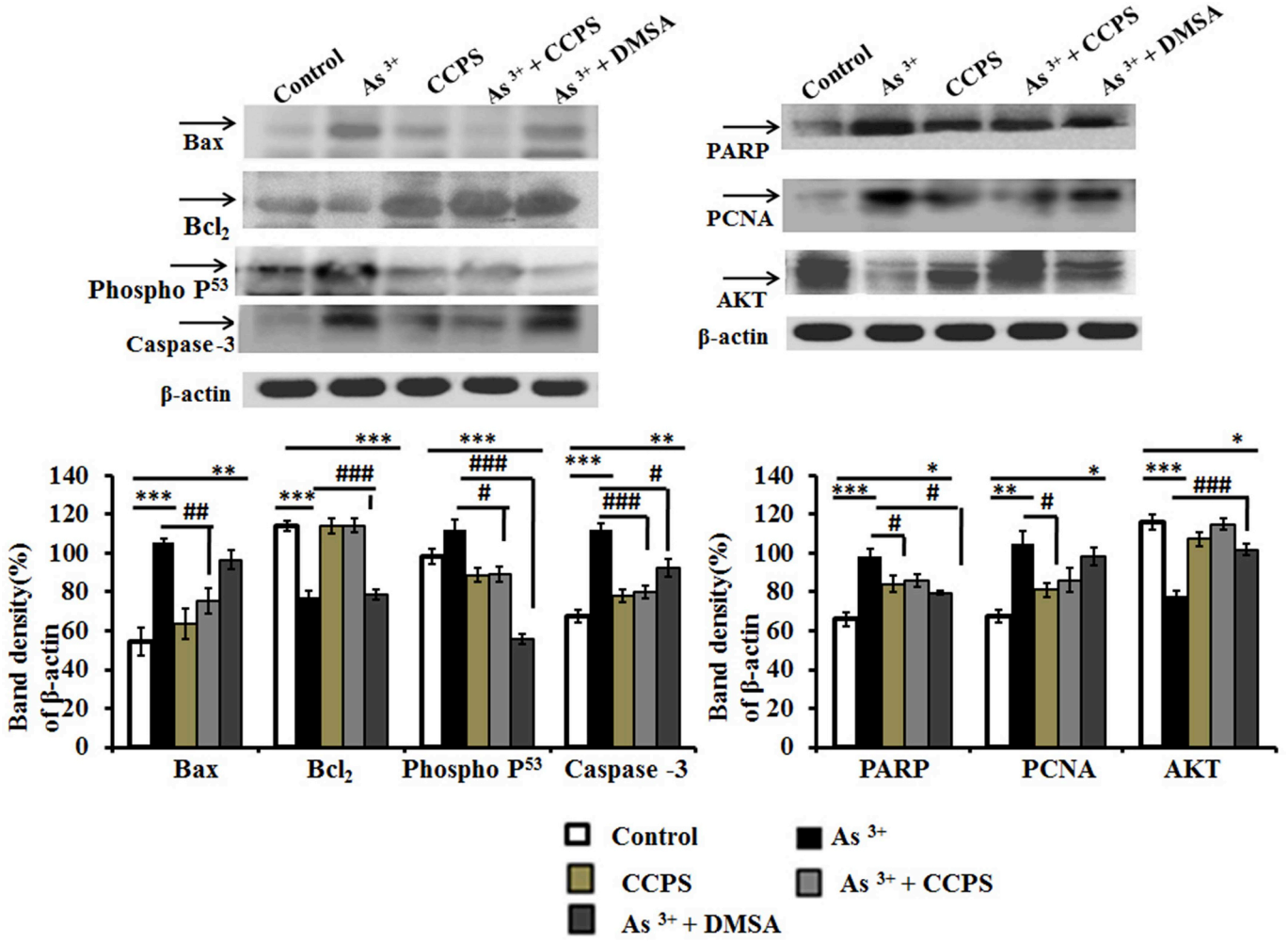

Fig. 9. Curative effects of CCPS on arsenic induced changes in activity of protein expression of Bax, caspase-3, Bcl_2, Phospho-p53, PCNA, PARP and AKT. The relative protein expression of β-actin, Bax, caspase-3, Bcl-2, Phospho-p53, PCNA, Parp and AKT respectively shown in Fig. 9. These results were represented as mean ± SE, N = 6 by ANOVA followed by post hoc Dunnett test. Significant differences were expressed as *p < 0.05, **p < 0.01 ***p < 0.001 with the control group and #p < 0.05, ##p < 0.01, ###p < 0.001 with the arsenic group.

reduced expression of these three enzymatic proteins in parallel with a rise in MDA and CD following the treatment of As^{3+} (Table 2 and Fig. 6) and these results is in agreement of our previous investigation where we found similar fashion of degradation of these antioxidant enzymes in arsenic fed rats (Dash et al., 2018).

CCPS has some positive action on antioxidant enzymes (Panda et al., 2015). Our results show that CCPS treatment significantly improves the As^{3+} induced uterine and ovarian damages *in vivo* and increased the above endogenous enzymatic antioxidant activities (Table 2 and Fig. 6). CCPS might exert its high radical scavenging activity and could scavenge NO and $\bullet O2^-$ through improving antioxidant enzyme activities and inhibit lipid peroxidation probably through the modulation of JNK3 kinase signal transmission (Gong et al., 2015). Our results indicate that CCPS reduces the MDA and CD level (Table-2) perhaps by replenishing the depleted GSH (Zeng et al., 2017).

Previous observation suggested that As^{3+} increased the serum LDH activity with a highly expressed LDH (Dash et al., 2018) which is consistent with our present findings (Fig. 7A and B). Our results explore that CCPS could reduce the LDH level (Fig. 7A and B) and act as a barrier against necrotic progression by maintaining the serum LDH. From here, we hypothesize that minimization of oxidative stress and necrosis by CCPS in As^{3+} ingested rats may possibly improve the uterine and ovarian disorders. This type of improvement may involve in two ways: direct or indirect action on ovarian and uterine tissues via estradiol. One is that CCPS may renovate the altered steroidogenesis and dysfunction of hypothalamic-pituitary–ovarian axis by maintaining LH and FSH in response to better steroidogenic enzyme activities and estradiol level during As^{3+} toxicity (Table 4). Another way, CCPS protects the ovarian-steroidogenic activity by its direct action in regulating the ER-α receptor (Table 4). Here, we describe that CCPS through oral route helps to recover the different stages of ovarian folliculogenesis and protects the ovary from follicular atresia (Fig. 11). So we postulate that CCPS might have a direct effect on ovarian follicle. The degeneration of uterine layers and loss of secretory glands are restored by the CCPS treatment (Fig. 11) and this may act as a safe guard in favoring the synthesis of estradiol for the maintenance of the uterine histo-architecture.

The transcription factor NF-κB belonging to the Rel family has an important role to regulate the development of different inflammatory diseases and different pro-inflammatory cytokines including TNF-α and IL-6. TNF-α is the most important inflammatory cytokine able to activate NF-κB, which can further up-regulate the expression of other inflammatory cytokines. This initiates a signaling cascade of activation. Oxidative stress is produced by the oxidation of cytotoxic free fatty acids results in the up-regulation of inflammatory cytokines (Ji et al., 2011). A high pro-inflammatory (IL-6 and TNF-α) and inflammatory cytokines (NF-κB) in arsenicated rats were supported by several authors. A higher concentration of MT-1 level is reflected in liver due to

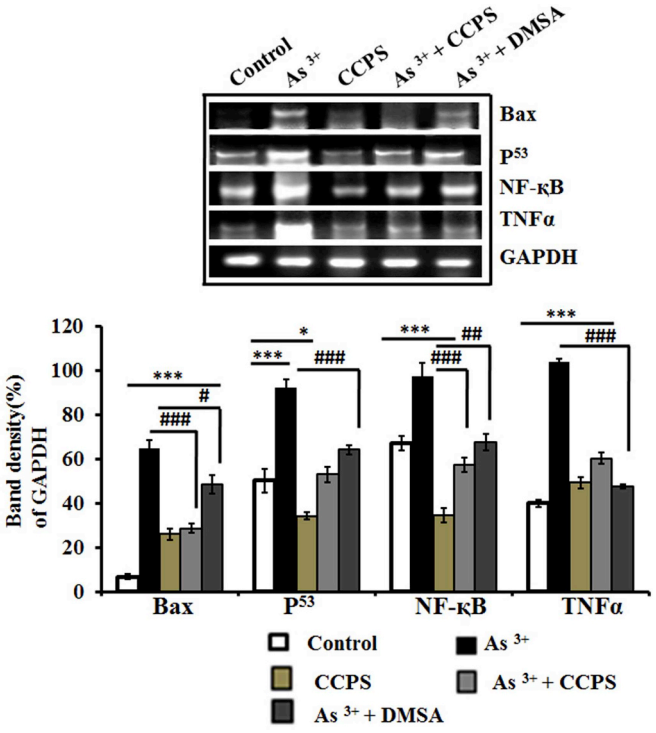

Fig. 10. Curative effects of CCPS on arsenic induced changes in activity of gene expression of Bax, Bcl-2, p53, NFκ-B and TNF-α. The relative protein expression of GAPDH, Bax, Bcl-2, p53, NFκ-B and TNF-α respectively shown in Fig. 10. These results were represented as mean ± SE, N = 6 by ANOVA followed by post hoc Dunnett test. Significant differences were expressed as *p < 0.05, ***p < 0.001 with the control group and at #p < 0.05, ##p < 0.01, ###p < 0.001 with the arsenic group.

As^{3+} toxicity in the present study (Fig. 8) as a primary defense system against oxidative stress. CCPS markedly down regulates the hepatic MT-1 level, both pro-inflammatory (TNF-α and IL-6) markers at the biochemical level (Fig. 8) and TNF-α at transcriptomic level by suppressing the gene expression of NF-κB (Fig. 10) and these results are consistent with the similar findings of other investigation (Mohammad, 2017). The cellular MT-1 primarily averts ROS generation during apoptosis via IKK-NF-κB pathway (Peng et al., 2007) as a homeostatic adjustment. NF-κB is the main regulator of oxidative stress, which regulates the several inflammatory genes which are responsible for dimerization, recognition, binding to DNA, and interactions with the different inhibitory proteins (Oliveira-Marques et al., 2009). Polysaccharide from *Momordica charantia* has a positive action on inflammatory markers as reported earlier (Mohammad, 2017). However, treatment with polysaccharide against As^{3+} inhibits the cytokines via NF-κB pathway in the way of improving inflammatory response of uterine tissues and hepatic MT-1 in arsenicated rats.

Our results explore an over expression of Bax at proteomic and genomic level, and suppression of Bcl-2 protein in response to As^{3+} (Figs. 9 and 10). The both pro-apoptotic protein Bax and anti-apoptotic protein Bcl-2 are regulated during arsenic driven apoptosis (Firdaus et al., 2018). Normally, high level of Bcl-2 protein expression prevents the integrity of the mitochondrial membrane which can protect the mitochondrial apoptosis factor and prevent the release of cytochrome-C from the apoptotic cells. However, As^{3+} toxicity increases ROS generation and arrests the mitochondrial function, cell cycle growth, and cell cycle and inhibits cell proliferation by inhibiting the activation of caspase-3 signaling pathway (Roussel and Barchowsky, 2000; Person et al., 2015). The mitochondrial functions are disrupted by oxidative stress which is under the control of anti-apoptotic Bcl-2 family genes and pro-apoptotic factors. This further activates the cytochrome-C directed release of activated caspase-3 (Hishita et al., 2001), leading to cell death. We suggest that ingestion of CCPS effectively inhibits As^{3+} induced apoptotic progression in uterine tissues by protecting the integrity of the mitochondrial membrane and terminating the release of the cytochrome-C from the mitochondria into cytoplasm by regulating the caspase cascade (Fig. 9).

The present study validates the protein expression of PKB/Akt in a rat. A low expression of uterine Akt protein in our study down regulates the expression of the Bcl-2 protein and up-regulates Bax at proteomic (Fig. 9) and genomic level (Fig. 10). This type of AKT signaling (Kovács et al., 2003) following CCPS post treatment in arsenicated rats inhibits apoptosis by improving estradiol level since estrogen substantiates the up-regulation of PKB/Akt signaling pathway via estradiol receptor (Kazi et al., 2009). A pro-apoptotic phase in response to As^{3+} and the occurrence of higher expression of p53 and inhibited expression of PKB/Akt were reflected. CCPS subsequently inhibits this pro-apoptotic stage by modulating a reverse antagonistic association between p53 and PKB/Akt (Fig. 9).

PCNA contributes as a bridge between cellular response to genotoxicity and leading strand synthesis of DNA replication (Strzalka and Ziemienowicz, 2011). PCNA complex proteins are critical in regulating

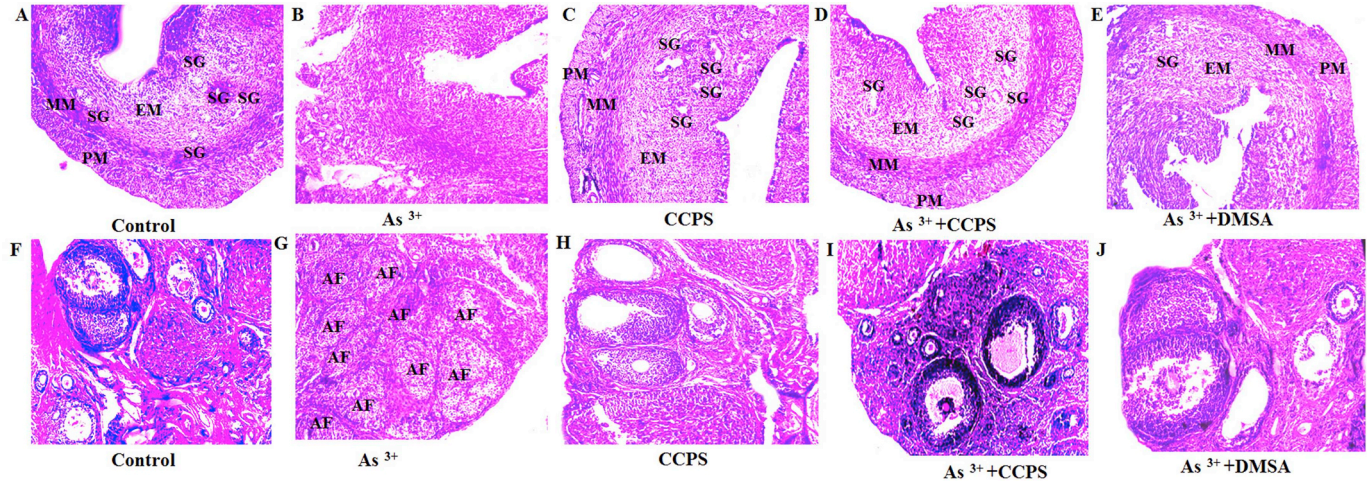

Fig. 11. Represent the curative effects of As^{3+} and CCPS on uterine and ovarian tissues. In uterine histo-architecture picture shows, loss of uterine layers (PM-Perimetrium, MM- Myometrium and, EM- Endometrium) and with loss of secretary glands (SG) but CCPS treatment induced arsenicated group recover the uterine layers specially secretary glands. In ovarian picture shows that, increased the number of atretic follicle. CCPS treatment showing reduced number of ovarian follicular artesia.

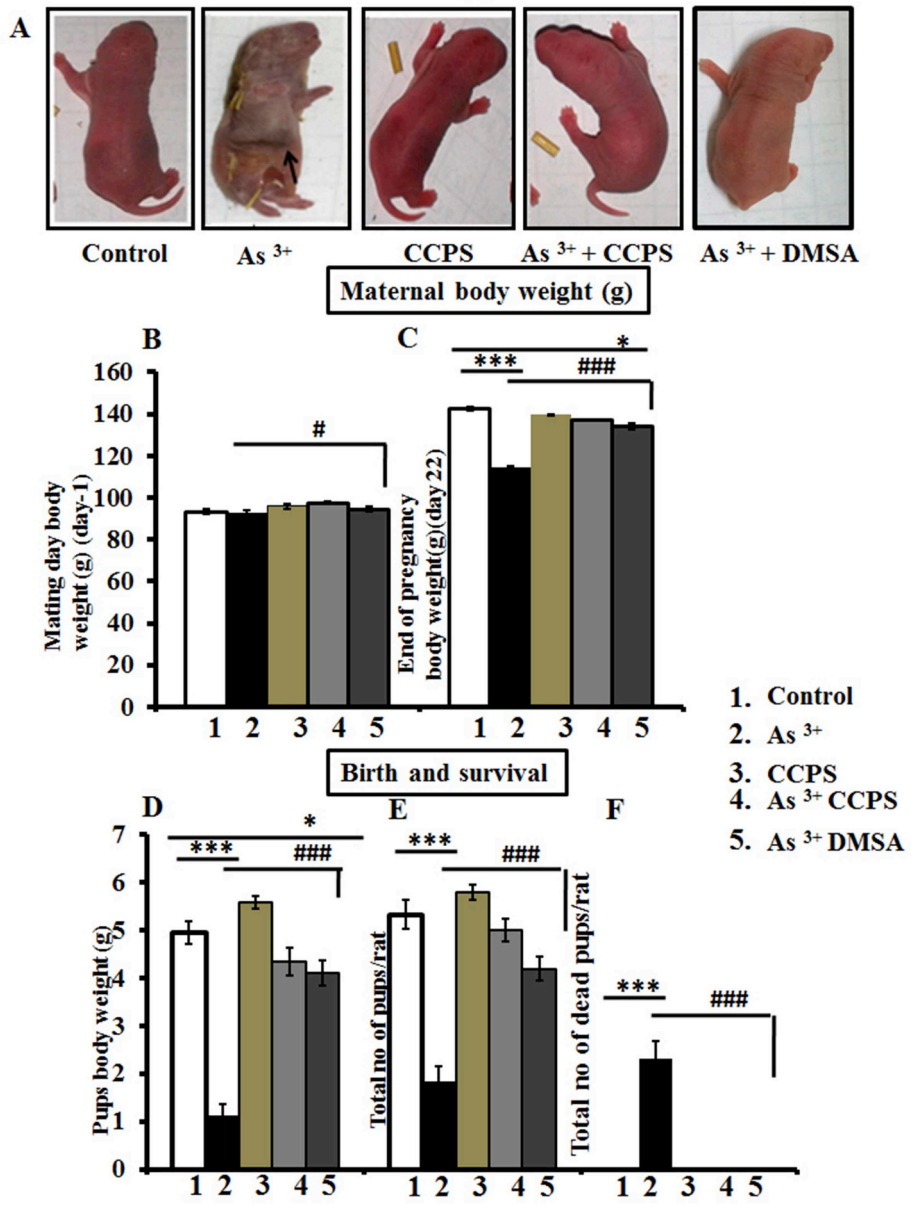

Fig. 12. A. Curative effects of CCPS on arsenic mediated female fertility status. CCPS treatment successfully delivers healthy pups without any deformities. Arrow indicates in arsenic ingested pregnant rats deliver unhealthy rats with deformities. **Figure 12B-12F**. CCPS ma**intain the pregnancy and a pup body weight and reduces the pup's dead rate at birth time**. These results were represented as mean ± SE, N = 6 by ANOVA followed by post hoc Dunnett test. Significant differences were expressed as *p < 0.05, ***p < 0.001 with the control group and #p < 0.05, ###p < 0.001 with the arsenic group.

MAP kinase and Akt pathways as well as apoptotic signaling. A highly expressed PCNA protein in arsenicated animals (Fig. 9) inhibits Akt signaling probably in association with AlkB homolog 2 PCNA interactive motifs (APIM peptide) (Olaisen et al., 2015). CCPS after As^{3+} treatment limits the extent of PCNA over expression and there by restrains the coverage of Akt signaling (Fig. 9). PARP is up-regulated in As^{3+} fed rats; this further induces the gene expression of IL-6, TNF-α via the activation of NF-κB by directly bound to it (Xueqing and Garg., 2011; Chiang et al., 2009). CCPS post-treatment in As^{3+} treated rats might be linked with PARP inhibition, minimization of the degree of inflammatory response of the cells by weakening NF-κB activation which finally modulates As^{3+} induced oxidative stress in uterine tissue (Fig. 9).

We further test the possibility of As^{3+} removal from the system through the involvement of SAM pool. We consider circulating B_{12}, folate and homocysteine as the components of SAM pool, though; in the present investigation, we did not consider the urinary arsenic speciation. Methionine cycle is the major mechanism for the detoxification of arsenic by modulating the methylation process with SAM as the methyl donor (Lin et al., 2002). Methyl donor is the most important factor in the arsenic bio-methylation process and arsenic bio-methylation. This is the major route of arsenic biotransformation cum elimination in mammals (Tice et al., 1997). Several studies reported that SAM level is reduced by arsenic toxicity and it alters some methylation process (Ramirez et al., 2005). Plasma level of vitamin B_{12} and folic acid are significantly reduced due to As^{3+} toxicity has been reported in the rats (Maity et al., 2018) and this report is consistent with our present findings. Folate acts as a co-factor in the generation of endogenous methionine which serves the methyl group in the methylation process (Henning et al., 1997). B_{12} acts conjointly with methionine synthase and 5-methyl tetrahydroflote to add the methyl group during the conversion of homocysteine to methionine (Refsum, 2001). The circulating levels of vitamin B_{12} and folic acid are important for the prevention of As^{3+} mediated tissue necrosis in a reproductive organ. In this study,

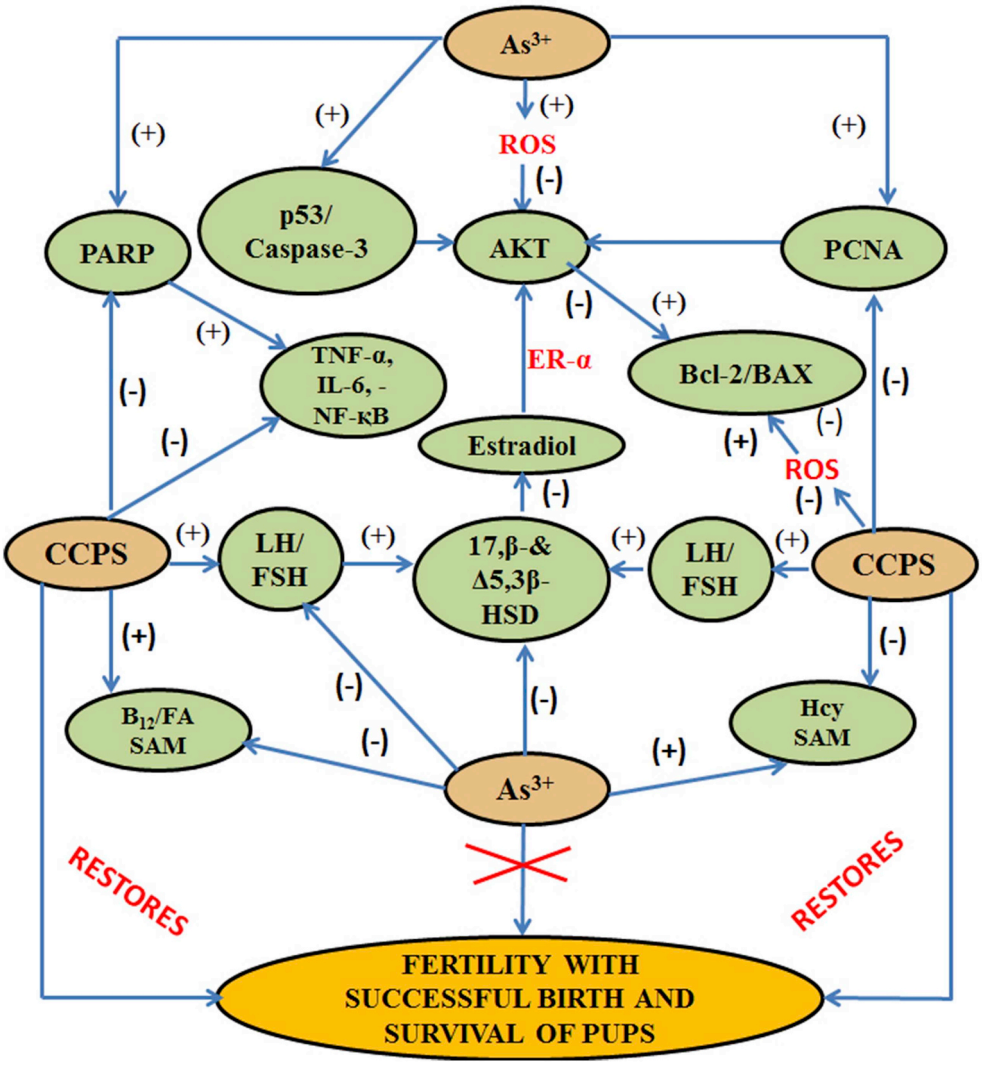

Fig. 13. Schematic diagram highlights the mechanism of CCPS action against arsenic induced toxicity. (+) and (-) sign denote stimulatory and inhibitory effect respectively.

significantly increased serum homocysteine is obtained in As^{3+} mediated rats and is corroborated with the findings of others (Maity et al., 2018).

An observation suggested that an elevated level of serum Hcy in As^{3+} mediated group degenerates ovarian follicles with follicular atresia (Kanakkaparambil et al., 2009). This might be possible that hyperhomocysteinemic condition suppresses follicular development and oocytes maturation and finally leads to infertility due to reduced estradiol production. We find that treatment with CCPS improves the circulating level of B_{12} and folic acid and limits the hyperhomocysteinemic condition in arsenic ingested rat because Hcy has lowering action on folic acid and B_{12} (Marcus et al., 2007). We assume that CCPS also maintains the estradiol production, follicular development by improving B_{12} and folic acid level in the way of the arsenic removal in methylated form.

Finally, on the basis of the above promising results we have been taken a further endeavor to test the fertility status of the female rats which were under the dietary consumption of CCPS in As^{3+} treatment phase. Successful fertility rate, pups survival and normal birth weight without deformities among the CCPS supplemented groups are observed in arsenicated rats (Fig. 12). These results confirm that CCPS could improve matting and fertility status by improving ovarian steroidogenesis and uterine antioxidant status via modulating the inflammatory, apoptotic, and necrotic biomarkers in As^{3+} treated rats at proteomic and/or genomic level.

5. Conclusions

We conclude that CCPS comprises of galacturonate acid residue that may interact with As^{3+}. CCPS orally mitigates and suppresses As^{3+} induced uterine and ovarian oxidative stress, inflammation and apoptosis by regulating Akt signaling pathway. Moreover, dietary CCPS improves fertility in female arsenicated rats with successful birth of the pups by maintaining the normal ovarian steroidogenic activity (Fig. 13).

Acknowledgements

This research work is partially supported by UGC Maulana Azad National Fellowship Scheme (MANF-2014-15-MUS-WES-35512). We are sincerely thankful to Prof. Sathees C. Raghavan, Department of Biochemistry, Indian Institute of Science, Bangalore, India for providing us technical help and infra structural facilities in his laboratory. We are sincerely thankful to Prof. S. Umapathy (Former HOD), Department of Inorganic and Physical Chemistry, Indian Institute of Science, Bangalore, India for providing us the FTIR spectroscopic facility. We are thankful to Prof. Ajay Kumar Mishra for his support in the imaging of scanning electron microscopy (SEM), Department of Chemistry and

Chemical Technology, Vidyasagar University, Midnapore, India. We are also thankful to Prof. Keshab Chandra Mondal, Department of Microbiology, Vidyasagar University, Midnapore, India for his support in this study.

Appendix A. Supplementary data

Supplementary data to this article can be found online at https://doi.org/10.1016/j.fct.2019.05.053.

References

Agrawal, S., Flora, G., Bhatnagar, P., Flora, S., 2014. Comparative oxidative stress, metallothionein induction and organ toxicity following chronic exposure to arsenic, lead and mercury in rats. Cell. Mol. Biol. 60 (2), 13–21 PMID: 24970117.

Ahmad, S.A., Sayed, M.H., Barua, S., Khan, M.H., Farquee, M.H., Jalil, A., Hadi, S.A., Talikder, H.K., 2001. Arsenic in drinking water and pregnancy outcomes. Environ. Health Perspect. 109, 629–631. https://doi.org/10.1289/ehp.01109629.

Bode, A.M., Dong, Z., 2002. The paradox of arsenic: molecular mechanisms of cell transformation and chemotherapeutic effects. Crit. Rev. Oncol. Hematol. 42 (1), 5–24 PMID: 11923065.

Brandt, R.B., Laux, J.E., Spainhour, S.E., Kline, E.S., 1987. Lactate dehydrogenase in rat mitochondria. Arch. Biochem. Biophys. 259 (2), 412–422 PMID: 3426237.

Carleton, A.B., Peters, R.A., Thompson, R.H.S., 1948. The treatment of arsenical dermatitis with dimercaptopropanol (BAL). Q. J. Med. 17, 49–79. https://doi.org/10.1172/JCI101733. PMID: 18905506.

Chao, C.Y., Huang, C.J., 2003. Bitter gourd (*Momordica charantia*) extract activates peroxisome proliferator-activated receptors and up regulates the expression of the acyl CoA oxidase gene in H4IIEC3 hepatoma cells. J. Biomed. Sci. 10 (6 Pt 2), 782–791. https://doi.org/10.1159/000073966.

Chatjigakis, A., Pappas, C., Proxenia, N., Kalantzi, O., Rodis, P., Polissiou, M., 1998. FT-IR spectroscopic determination of the degree of esterification of cell wall pectins from stored peaches and correlation to textural changes. Carbohydr. Polym. 37, 395–408. https://doi.org/10.1016/S0144-8617 (98)00057-5.

Chatterjee, A., Chatterjee, U., 2010. Arsenic abrogates the estrogen-signaling pathway in the rat uterus. Reprod. Biol. Endocrinol (8), 80. https://doi.org/10.1186/1477-7827-8-80.

Chattopadhyay, S., Maiti, S., Maji, G., Deb, B., Pan, B., Ghosh, D., 2010. Protective role of *Moringa oleifera* (sajina) seed on arsenic-induced hepatocellular degeneration in female albino rats. Biol. Trace Elem. Res. 142 (2), 200–212. https://doi.org/10.1007/s12011-010-8761-7.

Chaturvedi, P., 2009. Bitter melon protects against lipid peroxidation caused by immobilization stress in albino rats. Int. J. Vitam. Nutr. Res. 79 (1), 48–56. https://doi.org/10.1024/0300-9831.79.1.48.

Champlin, A.K., Dorr, D.L., Gates, A.H., 1973. Determining the stage of the estrous cycle in the mouse by the appearance of the vagina. Biol. Reprod. 8, 491–494. https://doi.org/10.1093/biolreprod/8.4.491.

Chawananorasest, K., Saengtongdee, P., Kaemchantuek, P., 2016. Extraction and characterization of Tamarind (Tamarind indica L.) seed polysaccharides (TSP) from three difference sources. Molecules 21 (6), 775. https://doi.org/10.3390/molecules21060775.

Cheng, H.R., Feng, S.L., Xue, X.J., Li, Q.Q., Zhou, Y.H., Ding, C.B., 2013. Structural characterization and antioxidant activities of polysaccharides extracted from Epimedium acuminatum, Carbohydr. Polymers 92 (1), 63–68. https://doi.org/10.1016/j.carbpol.2012.09.051.

Chiang, J., Shen, Y.C., Wang, Y.H., Hou, Y.C., Chen, C.C., Liao, J.F., Yu, M.C., Juan, C.W., Liou, K.T., 2009. Honokiol protects rats against eccentric exercise-induced skeletal muscle damage by inhibiting NF-kappa B induced oxidative stress and inflammation. Eur. J. Pharmacol. 610, 119–127. https://doi.org/10.1016/j.ejphar.2009.03.035.

Chokboribal, J., Tachaboonyakiat, W., Sangvanich, P., Ruangpornvisuti, V., Jettanacheawchankit, S., Thunyakitpisal, P., 2015. Deacetylation affects the physical properties and bioactivity of acemannan, an extracted polysaccharide from Aloe vera. Carbohydr. Polym. 133, 556–566. https://doi.org/10.1016/j.carbpol.2015.07.039.

Corsaro, M.M., De, C.C., Naldi, T., Parrilli, M., Tomás, J.M., Regué, M., 2005. 1 H and 13 C NMR characterization and secondary structure of the K2 polysaccharide of Klebsiella pneumoniae strain 52145. Carbohydr. Res. 340 (13), 2212–2217. https://doi.org/10.1016/j.carres.2005.07.006.

Cunha, A.P., Ribeiro, A.C., Ricardo, N.M., Oliveira, A.C., Dávila, L.S., Cardoso, J.H., Rodrigues, C.D., Azeredo, M.H., Silva, M.L., Brito, S.E., Filho, M.J., Rocha, M.T., Leal, K.L., Ricardo, M.N., 2017. Polysaccharides from Caesalpinia ferrea seeds–Chemical characterization and anti-diabetic effects in Wistar rats. Food Hydrocolloids 65, 68–76. https://doi.org/10.1016/j.foodhyd.2016.10.039.

Dash, M., Maity, M., Dey, M., Perveen, H., Khatun, S., Jana, L.R., Chattopadhyay, S., 2018. The consequence of NAC on sodium arsenite-induced uterine oxidative Stress. Toxicol. Rep 5, 278–287. https://doi.org/10.1016/j.toxrep.2018.02.003.

Deeyai, P., Suphantharika, M., Wongsagonsup, R., Dangtip, S., 2013. Characterization of modified tapioca starch in atmospheric argon plasma under diverse humidity by FTIR spectroscopy. Chin. Phys. Lett. 30, 018103. https://doi.org/10.1088/0256-307X/30/1/018103.

Devasagayam, T.P., Boloor, K.K., Ramasarma, T., 2003. Methods for estimating lipid peroxidation: an analysis of merits and demerits. Indian J. Biochem. Biophys. 40, 300–308 PMID: 22900323.

El-Zoghbi, M., Sitohy, M.Z., 2001. Mineral absorption by albino rats as affected by some types of dietary pectins with different degrees of esterification. Nahrung 45 (2), 114–117. https://doi.org/10.1002/1521-3803(20010401)45:2<114::AID-FOOD114>3.0.CO;2-G.

Firdaus, F., Zafeer, M.F., Anis, E., Ahmad, M., Afzal, M., 2018. Ellagic acid attenuates arsenic induced neuro-inflammation and mitochondrial dysfunction associated apoptosis. Toxicol. Rep 5, 411–417. https://doi.org/10.1016/j.toxrep.2018.02.017.

Gong, J., Sun, F., Li, Y., Zhou, X., Duan, Z., Duan, F., Zhao, L., Chen, H., Qi, S., Shen, J., 2015. *Momordica charantia* polysaccharides could protect against cerebral ischemia/reperfusion injury through inhibiting oxidative stress mediated c-Jun N-terminal kinase 3 signaling pathway. Neuropharmacology 91, 123–134. https://doi.org/10.1016/j.neuropharm. 2014.11.020.

Hadwan, M.H., 2016. New method for assessment of serum catalase activity. Indian. J. Sci. T. echnol 9, 1–5. https://doi.org/10.17485/ijst/2016/v9i4/80499.

Hartley-Whitaker, J., Ainsworth, G., Meharg, A., 2001. Copper and arsenic induced oxidative stress in holcuslanatus L. Clones with differential sensitivity. Plant Cell Environ. 24, 713–722. https://doi.org/10.1046/j.0016-8025.2001.00721.x.

Henning, S.M., Swendseid, M.,E., Coulson, W.F., 1997. Male rats fed methyl-and folate-deficient diets with or without niacin develop hepatic carcinomas associated with decreased tissue NAD concentrations and altered poly (ADP-ribose) polymerase activity. J. Nutr. 127 (1), 30–36. https://doi.org/10.1093/jn/127.1.30.

Hishita, T., Tada-Oikawa, S., Tohyama, K., Miura, Y., Nishihara, T., Tohyama, Y., Yoshida, Y., Uchiyama, T., Kawanishi, S., 2001. Caspase-3 activation by lysosomal enzymes in cytochrome c-independent apoptosis in myelodysplastic syndrome-derived cell line P39. Cancer. Res. 61 (7), 2878–2884 PMID:11306462.

Inns, R.H., Rice, P., Bright, J.E., Marrs, T.C., 1990. Evaluation of the efficacy of dimercapto chelating agents for the treatment of systemic organic arsenic poisoning in rabbits. Hum. Exp. Toxicol. 9, 215–220. https://doi.org/10.1177/096032719000900403.

Jarabak, J., Adams, J.A., Williams-Ashman, H.G., Talalay, P., 1962. Purification of 17β-hydroxysteroid dehydrogenase function. J. Biol. Chem. 237, 345–357 PMID: 14451294.

Ji, G., Yang, Q., Hao, J., Guo, L., Chen, X., Hu, J., 2011. Anti-inflammatory effect of genistein on non-alcoholic steatohepatitis rats induced by high fat diet and its potential mechanisms. Int. Immunopharmacol. 11 (6), 762–768. https://doi.org/10.1016/j.intimp.2011.01.036.

Jilka, C., Strifler, B., Fortner, G.W., Hays, E.F., Takemoto, D.J., 1983. In vivo antitumor activity of the bitter melon *(Momordica charantia*). Cancer Res. 43 (11), 5151–5155 PMID: 6616452.

Kanakkaparambil, R., Singh, R., Li, D., Webb, R., Sinclair, K.D., 2009. B-vitamin and homocysteine status determines ovarian response to gonadotropin treatment in sheep. Biol. Reprod. 80 (4), 743–752.

Kang, J.H., Yun, S.I., Park, M.H., Park, J.H., Jeong, S.Y., Park, H.O., 2013. Anti-obesity effect of *Lactobacillus gasseri* BNR17 in high-sucrose diet-induced obese mice. PLoS One 8, e54617. https://doi.org/10.1371/journal.pone.0054617.

Kazi, A.A., Molitoris, K.H., Koos, R.D., 2009. Estrogen rapidly activates the PI3K/AKT pathway and hypoxia-inducible factor 1 and induces vascular endothelial growth factor A expression in luminal epithelial cells of the rat uterus. Biol. Reprod. 81 (2), 378–387. https://doi.org/10.1095/biolreprod.109.076117.

Khatun, S., Maity, M., Perveen, H., Dash, M., Chattopadhyay, S., 2018. Spirulina platensis ameliorates arsenic mediated uterine damage and ovarian steroidogenic disorder. FACETS 3, 736–753. https://doi.org/10.1139/facets-2017-0099.

Kim, Y.J., Kim, J.M., 2015. Arsenic toxicity in male reproduction and development. Dev. Reprod 19 (4), 167–180. https://doi.org/10.12717/DR.2015.19.4.167.

Kovács, K.A., Lengyel, F., Környei, J.L., Vértes, Z., Szabó, I., Sümegi, B., Vértes, M., 2003. Differential expression of Akt/protein kinase B, Bcl-2 and Bax proteins in human leiomyoma and myometrium. J. Steroid Biochem. Mol. Biol. 87, 233–240 PMID: 14698203.

Kumar, A., 2012. Effect of simuastation on paraxonase 1 (PON1) activity and oxidation stress. In: Kumar, A. (Ed.), Significance of Lipid Profile Assay as Diagnostic and Prognostic Tool, Create Space Independent Publishing Platform, California, pp. 105–109.

Kumar, R., Balaji, S., Sripriya, R., Nithya, N., Uma, T.S., Sehgal, P.K., 2010. In vitro evaluation of antioxidants of fruit extract of *Momordica charantia* L. on fibroblasts and keratinocytes. J. Agric. Food Chem. 58 (3), 1518–1522. https://doi.org/10.1021/jf9025986.

Lewis, A., Du, J., Liu, J., RitchieJ, M., Oberley, L.W., Cullen, J.J., 2006. Metastatic progression of pancreatic cancer: changes in antioxidant enzymes and cell growth. Clin. Exp. Metastasis 22, 523–532. https://doi.org/10.1007/s10585-005-4919-7.

Lin, S., Shi, Q., Nix, F.B., Styblo, M., Beck, M.A., Herbin-Davis, K.M., Hall, L.L., Simeonsson, J.B., Thomas, D.J., 2002. A novel S-adenosyl-L-methionine:arsenic (III) methyltransferase from rat liver cytosol. J. Biol. Chem. 277 (13), 10795–10803. https://doi.org/10.1074/jbc.M110246200.

Liu, J., Du, J., Zhang, Y., Sun, W., Smith, B.J., Oberley, L.W., Cullen, J.J., 2006. Suppression of the malignant phenotype in pancreatic cancer by the over expression of phospholipid hydroperoxide glutathione peroxidase. Hum. Gene Ther. 17, 105–116. https://doi.org/10.1089/hum.2006.17.105.

Maiti, S., Chattopadhyay, S., Acharyya, N., Deb, B., Hati, A.K., 2014. *Emblica officinalis* (amla) ameliorates arsenic-induced liver damage via DNA protection by antioxidant systems. Mol. Cell. Toxicol 10, 75–82. https://doi.org/10.1007/s13273-014-0009-8.

Maity, M., Perveen, H., Dash, M., Jana, S., Khatun, S., Dey, A., 2018. Arjunolic acid improves the serum level of vitamin B_{12} and folate in the process of the attenuation of arsenic induced uterine oxidative stress. Biol. Trace Elem. Res. 182 (1), 78–90. https://doi.org/10.1007/s12011-017-1077-0.

Maji, P.K., Sen, I.K., Behera, B., Maiti, T.K., Mallick, P., Sikdar, S.R., 2012. Structural characterization and study of immune enhancing properties of a glucan isolated from

a hybrid mushroom of Pleurotus Florida and Lentinulaedodes. Carbohydr. Res. 358, 110–115. https://doi.org/10.1016/j.carres.2012.06.017.
Manrique, G.D., Lajolo, F.M., 2002. FT-IR spectroscopy as a tool for measuring degree of methyl esterification in pectins isolated from ripening papaya fruit. Postharvest Biol. Technol. 25, 99–107. https://doi.org/10.1016/S0925-5214(01)00160-0.
Marcus, J., Sarnak, M.J., Menon, V., 2007. Homocysteine lowering and cardiovascular disease risk: lost in translation. Can. J. Cardiol. 23 (9), 707–710 PMCID:PMC2651913.
Mieyal, J.J., Gallogly, M.M., Qanungo, S., Sabens, E.A., Shelton, M.D., 2008. Molecular mechanisms and clinical implications of reversible protein S-glutathionylation. Antioxid. Redox. Rignal 10, 1941–1988. https://doi.org/10.1089/ars.2008.2089.
Mohammad, R., 2017. *Momordica charantia* polysaccharides ameliorate oxidative stress, hyperlipidemia, inflammation, and apoptosis during myocardial infarction by inhibiting the NF-κB signaling pathway. Int. J. Biol. Macromol. 97, 544–551. https://doi.org/10.1016/j.ijbiomac.2017.01.074.
Mohammad, R., Ahmad, A., Jan, B.L., Alkharfy, K.M., Ansari, M.A., Mohsin, K., Jenoobi, F.A., Al-Mohizea, A., 2016. *Momordica charantia* polysaccharides mitigate the progression of STZ induced diabetic nephropathy in rats. Int. J. Biol. Macromol. 91, 394–399. https://doi.org/10.1016/j.ijbiomac.2016.05.090.
Olaisen, C., Müller, R., Nedal, A., Otterlei, M., 2015. PCNA-interacting peptides reduce Akt phosphorylation and TLR-mediated cytokine secretion suggesting a role of PCNA in cellular signaling. Cell. Signal. 27 (7), 1478–1487. https://doi.org/10.1016/j.cellsig.2015.03.009.
Oliveira-Marques, V., Marinho, H.S., Cyrne, L., Antunes, F., 2009. Role of hydrogen peroxide in NF-kappa B activation: from inducer to modulator. Antioxidants Redox Signal. 11 (9), 2223–2243. https://doi.org/10.1089/ars.2009.2601.
Paglia, D.E., Valentine, W.N., 1967. Studies on quantitative and qualitative characterization of erythrocyte glutathione peroxidise. J. Lab. Clin. Med. 70, 158–169 PMID:6066618.
Pan, J.S., Hong, M.Z., Ren, J.L., 2009. Reactive oxygen species: a double-edged sword in oncogenesis. World J. Gastroenterol. 14, 1702–1707. https://doi.org/10.3748/wjg.15.1702.
Panda, B.C., Mondal, S.K., Devi, P.S., Maiti, T.P., Khatua, S., Acharya, K., 2015. Pectic polysaccharide from the green fruits of *Momordica charantia* (Karela): structural characterization and study of immune enhancing and antioxidant properties. Carbohydr. Res. 401https://doi.org/10.1016/j.carres.2014.10.015. 24–3.
Pattichis, K., LoucaL, L., Glover, V., 1994. Quantitation of soluble superoxide dismutase in rat striata, based on the inhibition of nitrite formation from hydroxyl ammonium chloride. Anal. Biochem. 221, 428–431. https://doi.org/10.1006/abio.1994.1441.
Paula, R., Heatley, F., Budd, P.M., 1998. Characterization of Anacardium occidentale exudates polysaccharide. Polym. Int. 45 (1), 27–35. https://doi.org/10.1002/(SICI)1097-0126(199801)45:1<27::AID-PI900>3.0.CO;2-9.
Peng, H., Wang, N., Hu, Z., Yu, Z., Liu, Y., Zhang, J., Ruan, R., 2012. Physicochemical characterization of hemicelluloses from bamboo (Phyllostachys pubescens Mazel) stem. Ind. Crops Prod. 37 (1), 41–50. https://doi.org/10.1016/j.indcrop.2011.11.031.
Peng, Z., Peng, L., Fan, Y., Zandi, E., Howard, G., Shertzer, H.G., Xia, Y., 2007. A critical role for IKKE in metallothionein-1 expression and protection against arsenic toxicity. J. Biol. Chem. 282 (29), 21487–21496. https://doi.org/10.1074/jbc.M702510200.
Person, R.J., Ngalame, N.N., Makia, N.L., Bell, M.W., Waalkes, M.P., Tokar, E.J., 2015. Chronic inorganic arsenic exposure in vitro induces a cancer cell phenotype in human peripheral lung epithelial cells. Toxicol. Appl. Pharmacol. 286 (1), 36–43. https://doi.org/10.1016/j.taap.2015.03.014.
Perveen, H., Dash, M., Khatun, S., Maity, M., Islam, S.S., Chattopadhyay, S., 2017. Electrozymographic evaluation of the attenuation of arsenic induced degradation of hepatic SOD, catalase in an in vitro assay system by pectic polysaccharides of *Momordica charantia* in combination with curcumin. Biochem. Biophys. Rep 11, 64–71. https://doi.org/10.1016/j.bbrep.2017.06.002.
Ramirez, T., Garcia-Montalvo, V., Wise, C., Cea-Olivares, R., Poirier, L.A., Herrera, L.A., 2005. S-adenosyl-L-methionine is able to reverse micronucleus formation induced by sodium arsenite and other cytoskeleton disrupting agents in cultured human cells. Mutat. Res. 528 (1–2), 61–74 PMID:12873724.
Raqib, R., Ahmed, S., Sultana, R., Wagatsuma, Y., Mondal, D., Hoque, A.M., 2009. Effects of in utero arsenic exposure on child immunity and morbidity in rural Bangladesh. Vahter. M. Toxicol. Lett 185 (3), 197–202. https://doi.org/10.1016/j.toxlet.2009.01.001.
Refsum, H., 2001. Folate, vitamin $B1_2$ and homocysteine in relation to birth defects and pregnancy outcome. Br. J. Nutr. 85, S109–S113. https://doi.org/10.1049/BJN2000302.
Robitaille, L., John, L., 2016. A simple method for plasma total vitamin C analysis suitable for routine clinical laboratory use. Nutr. J. 15, 40. https://doi.org/10.1186/s12937-016-0158-9.
Romdhanea, M.B., Haddara, A., Ghazala, I., Jeddou, K.B., Helbert, C.B., Chaabouni, S.E., 2017. Optimization of polysaccharides extraction from watermelon rinds: structure, functional and biological activities. Food Chem. 216, 355–364. https://doi.org/10.1016/j.foodchem.2016.08.056.
Roussel, R.R., Barchowsky, A., 2000. Arsenic inhibits NF-kappa B-mediated gene transcription by blocking I kappa B kinase activity and I kappa B alpha phosphorylation and degradation. Arch. Biochem. Biophys. 377 (1), 204–212. https://doi.org/10.1006/abbi.2000.1770.
Santhiya, D., Subramanian, S., Natarajan, K.A., Colloid, I.J., 2002. Surface chemical studies on sphalerite and galena using extracellular polysaccharides isolated from Bacillus polymyxa. Science 256 (2), 237–248 PMID:12573627.
Strzalka, W., Ziemienowicz, A., 2011. Proliferating cell nuclear antigen (PCNA): a key factor in DNA replication and cell cycle regulation. Ann. Bot. 107 (7), 1127–1140. https://doi.org/10.1093/aob/mcq243.
Talalay, P., 1962. Hydroxysteroid dehydrogenase. In: Colowick, S.P., Kaplan, N.O. (Eds.), Methods in Enzymology. Academic Press, New York, pp. 512–516.
Tan, S., Gao, B., Tao, Y., Guo, J., Su, Z., 2014. Antiobese effects of capsaicin-chitosan microsphere (CCMS) in obese rats induced by high fat diet. J. Agric. Food Chem. 62 (8), 1866–1874. https://doi.org/10.1021/jf4040628.
Tice, R.R., Yager, J.W., Andrews, P., Crecelius, E., 1997. Effect of hepatic methyl donor status on urinary excretion and DNA damage in B6C3F1 mice treated with sodium arsenite. Mutat. Res. 386 (3), 315–334 PMID:9219569.
Usoh, I.F., Akpan, E.J., Etim, E.O., Farombi, E.O., 2005. Antioxidant actions of dried flower extracts of Hibiscus sabdariffa L. On sodium arsenite-induced oxidative stress in rats. Pakistan J. Nutr. 4 (3), 135–141. https://doi.org/10.3923/pjn.2005.135.141.
Weydert, C.J., Cullen, J.J., 2010. Measurement of superoxide dismutase, catalase, and glutathione peroxidase in cultured cells and tissue. Nat. Protoc. 5 (1), 51–66. https://doi.org/10.1038/nprot.2009.197.
Xu, X., Chen, P., Wang, Y., Zhang, L., 2009. Chain conformation and rheological behavior of an extracellular hetero polysaccharide Erwinia gum in aqueous solution. Carbohydr. Res 5 344 (1), 113–119. https://doi.org/10.1016/j.carres.2008.10.009.
Xueqing, B., Garg, N.J., 2011. Signaling mechanism of poly (ADP-Ribose) polymerase-1 (PARP-1) in inflammatory diseases. Am. J. Pathol. 178 (3), 946–955. https://doi.org/10.1016/j.ajpath.2010.12.004.
Zeng, Q., Ko, C.H., Siu, W.S., Li, L.F., Han, X.Q., Yang, L., 2017. Polysaccharides of Dendrobium officinale Kimura & Migo protect gastric mucosal cell against oxidative damage-induced apoptosis in vitro and in vivo. J. Ethnopharmacol. 208, 214–224. https://doi.org/10.1016/j.jep.2017.07.006.
Zhang, C., Chen, H., Bai, W., 2018. Characterization of *Momordica charantia* L. polysaccharide and its protective effect on pancreatic cells injury in STZ-induced diabetic mice. Int. J. Biol. Macromol. 115, 45–52. https://doi.org/10.1016/j.ijbiomac.2018.04.039.
Zhang, C., Ling, B., Liu, J., Wang, G., 2000. Toxic effect of fluoride-arsenic on the reproduction and development of rats. Wei Sheng Yan Jiu 29 (3), 138–140 PMID:12725053.